# Novel Covalent Adaptable Networks (CANs) of Ethylene/1-Octene Copolymers (EOCs) Made by Free-Radical Processing: Comparison of Structure-Property Relationships of EOC CANs with EOC Thermosets

| | |
|---|---|
| Journal: | *Polymer Chemistry* |
| Manuscript ID | PY-ART-04-2023-000444.R1 |
| Article Type: | Paper |
| Date Submitted by the Author: | 05-Jul-2023 |
| Complete List of Authors: | Chen, Boran; Northwestern University<br>Fenimore, Logan; Northwestern University,<br>Chen, Yixuan; Northwestern University<br>Barbon, Stephanie; The Dow Chemical Company<br>Brown, Hayley; The Dow Chemical Company<br>Auyeung, Evelyn; The Dow Chemical Company<br>Shan, Colin; The Dow Chemical Company<br>Torkelson, John; Northwestern University, |
| | |

# Novel Covalent Adaptable Networks (CANs) of Ethylene/1-Octene Copolymers (EOCs) Made by Free-Radical Processing: Comparison of Structure-Property Relationships of EOC CANs with EOC Thermosets

**Boran Chen,[a,#] Logan M. Fenimore,[a,#] Yixuan Chen,[a] Stephanie Barbon,[b] Hayley Brown,[c] Evelyn Auyeung,[c] Colin Li Pi Shan,[c] John M. Torkelson[a,d,*]**

[a]Department of Chemical and Biological Engineering, Northwestern University, Evanston, IL 60208 USA

[b]The Dow Chemical Company, Midland, MI 48674 USA

[c]The Dow Chemical Company, Lake Jackson, TX 77566 USA

[d]Department of Materials Science and Engineering, Northwestern University, Evanston, IL 60208 USA

[#]co-first authors *corresponding author: j-torkelson@northwestern.edu

**Abstract:** Ethylene-based copolymers such as ethylene/1-octene copolymers (EOCs) are commonly used in blends for thermoplastic elastomers, foams, and consumer articles. These blends may be permanently cross-linked to enhance elasticity at the expense of their recyclability. Literature studies on structure-property relationships between precursor EOCs and their permanently cross-linked counterparts (EOCXs) are conflicting. Additionally, few studies have sought to overcome the recyclability issues of EOCXs by incorporating dynamic bonds into their structures to produce EOC covalent adaptable networks (EOC CANs). Here, we synthesized

several EOCXs and EOC CANs from EOCs of varying 1-octene content and melt flow index (MFI) using a simple, radical-based reactive process. The EOC CANs are made capable of dialkylamino disulfide dynamic covalent chemistry by incorporation of dissociative bis(2,2,6,6-tetramethyl-4-piperidyl methacrylate) disulfide (BiTEMPS methacrylate) cross-links during reactive processing. Increasing the 1-octene content and MFI in EOCs generally reduces the grafting efficiency of BTMA and cross-link density in EOCXs and EOC CANs. Decreasing cross-link density in EOC CANs results in greater losses of cross-link density with increasing temperature from the dissociative BiTEMPS methacrylate cross-links as well as shorter stress relaxation times. Stress relaxation activation energies in EOC CANs generally align with previously reported bond dissociation energies and activation energies associated with BiTEMPS-related molecules and CANs. While EOCXs could not be reprocessed into healed films, our EOC CANs are reprocessable and fully recover their cross-link densities and thermomechanical properties within error after successive compression molding cycles.

## 1. Introduction

Crystallinity in polyethylene (PE) provides advantageous qualities such as strength, stiffness, and chemical resistance.[1,2] Interlamellar amorphous regions add toughness and environmental stress crack resistance.[3] Depending on the distribution of short-chain branching in these amorphous regions, properties in PE and PE-like materials can vary from plastic to elastomeric.[4-6] To toughen amorphous regions further, ethylene is often copolymerized with α-olefin comonomers that increase short-chain branching in amorphous phases.[7-10] These low-cost, commercial copolymers are most often produced using Ziegler-Natta or metallocene catalysis methods which can control the breadths of molecular weight, composition, and short-chain branching distributions.[9,11]

1-Octene is a common α-olefin comonomer in commercial ethylene-based thermoplastic elastomers. Depending on the catalysis method, random and block microstructures are possible in ethylene/1-octene copolymers (EOCs). In the early 1990s, metallocene catalysis typical in ethylene copolymer syntheses evolved after the discovery of single-site constrained geometry catalyst

technology.[12,13] Polyolefins that were once unattainable via conventional Ziegler-Natta or metallocene catalysis saw rapid development and production, e.g., random EOCs with narrow short-chain branching distributions.[12] Random EOCs feature fringed micellar crystals from the crystallizable ethylene that act as physical cross-links between rubbery, amorphous regions containing ethylene and 1-octene repeat units.[14,15] These strong, physical cross-links provide EOCs with elasticity and strength, and EOCs are desirable as low-cost impact modifiers and toughenersin thermoplastic elastomers, foams, and shape memory polymers for applications like footwear, cushioning, and catheters.[16-23] EOCs are common components in blends with other polymers such as polypropylene (PP),[24-28] ethylene propylene diene monomer (EPDM) rubber,[29-32] ethylene-vinyl acetate copolymer (EVA),[33-35] and polydimethylsiloxane (PDMS).[36,37] Like PE, EOCs and their blends may be vulcanized or covalently cross-linked using radical initiators such as peroxides to enhance properties like elasticity and temperature resistance.[18,38-44] Light vulcanization, or covalent cross-linking below the percolation limit, maintains the processability of EOCs and their blends at high temperature but leaves them susceptible to irreversible deformation from creep. In contrast, permanently cross-linking such EOCs above the percolation limit helps to resist this deformation and enhance elasticity further at the expense of processability.[45]

Studies agree that EOCs offer opportunities to establish structure-property relationships as functions of single variables like 1-octene content and molecular weight.[6,14,46,47] However, because of their intricate microstructures, general properties of EOCs are not fully understood, and the understanding of EOC cross-linking is incomplete. While deriving structure-property relationships in random EOCs is more straightforward than in multi-block EOCs, studies on cross-linked random EOCs sometimes draw conflicting conclusions after varying several parameters at once.[46] Nicolás et al.[48] reported that increasing 1-octene content in random EOCs caused greater chain scission during peroxide cross-linking, leading to decreased gel contents. Msakni et al.[41] disputed this reasoning by noting that the random EOC with higher 1-octene content in Nicolás et al.[48] also had a higher melt flow index (MFI) that negatively contributed to cross-linking. They backed up their point by demonstrating that increasing MFI in their random EOCs of nearly identical 1-octene

contents led to decreased gel contents and rubbery plateau shear moduli after peroxide cross-linking.[41] They also found that varying 1-octene contents of random EOCs with identical MFIs led to negligible differences in gel contents and rubbery plateau shear moduli after peroxide cross-linking.[41] Svoboda et al.[17] later reported completely opposite results of Msakni et al.[41] Gel contents and other cross-linking parameters in their peroxide-cross-linked random EOCs increased with decreasing 1-octene (at constant MFI) as well as increasing MFI (at nearly constant 1-octene content), a more puzzling result.[17] Padmanabhan et al.[37] later corroborated some findings of Svoboda et al.[17], e.g., that decreasing 1-octene in random EOCs increases gel contents and other cross-linking parameters. They cite the initiator bulkiness and the higher concentration of sterically hindering branches in random EOCs of greater 1-octene content as factors negatively affecting macroradical formation.[37] Yet, their claims are complicated by the larger MFI of their random EOC of greater 1-octene content because a larger MFI is expected to decrease peroxide cross-linkability of random EOCs. Greater clarity on the understanding of EOC cross-linking is warranted given their growing prevalence and the contrasting literature reports.

As mentioned, EOCs with permanent cross-links above the percolation limit are not processable at high temperatures. Incorporating dynamic covalent bonds into EOCs could be a solution to this sacrifice in recyclability. When dynamic covalent bonds are integrated into polymers as cross-links, covalent adaptable networks (CANs), also called dynamic covalent polymer networks (DCPNs), are formed.[49-56] Dynamic bonds in CANs undergo reversible reactions that reconfigure their chemical arrangements and allow for local chain mobility upon the input of a stimulus such as heat. From this local chain mobility, CANs may be recycled via melt-state processing.[53-55] Associative dynamic chemistries such as transesterification,[57-59] transamination,[60-62] boronic ester exchange,[63-65] and disulfide exchange[66-68] involve the simultaneous formation and breaking of bonds. Associative CANs, or vitrimers,[56,69,70] maintain their theoretical cross-link densities; the total number of bonds at any point remains unchanged during exchange.[56,69,70] Dissociative dynamic chemistries such as the Diels-Alder reaction,[49,71-75] alkoxyamine chemistry,[76-78] hindered urea exchange,[79-82] and dialkylamino disulfide chemistry[83-

[88] involve the reversion of dynamic bonds with the input of a stimulus and their reassociation after removal of the stimulus.[60] With increasing temperature, the number of dissociating dynamic bonds contributing to network behavior decreases.[60] Some CANs exhibit several concurrent dynamic chemistries.[89-94] Owing to their dynamic bonds, CANs function as conventional thermosets exhibiting cross-linked features at elevated use temperatures, such as creep resistance and compressive recovery, and have the potential to be recycled, like conventional thermoplastics, via melt processing. Many thermoset elastomers are cross-linked with sulfur and peroxide systems and are commonly used in durable applications for automotive weather seals, tires, roofing membranes, and many other general rubber goods that require long term durability that can resist deformation at elevated temperatures. CANs have potential to offer a circular solution to resolve the end-of-life recovery and management of thermoset polyolefin elastomers.

Post-polymerization modifications to graft small molecules onto polymers are growing in popularity as methods to upcycle polyolefins into CANs with enhanced properties and reprocessability.[52,63,72,73,88,95-114] We recently reported a simple, catalyst-free procedure to upcycle PE into reprocessable PE CANs capable of dialkylamino disulfide dynamic covalent chemistry by incorporating bis(2,2,6,6-tetramethyl-4-piperidyl methacrylate) disulfide (BiTEMPS methacrylate, or BTMA) as a dynamic cross-linker through melt-state reactive processing.[88] Despite efforts to produce polyolefin CANs, EOC-based CANs have been seldomly reported, and no report discusses their structure-property relationships after dynamic covalent cross-linking. To the best of our knowledge, three patents[115-117] report formulations including random or multi-block EOCs in CANs, and several articles[118-123] report EOC-based CANs, all since 2019. There is no report of EOC CANs synthesized exclusively by free-radical methods, and the unclear or limited information on factors, such as 1-octene content and MFI, influencing EOC permanent and dynamic covalent cross-linking justifies further study.

Herein, we synthesized several permanently cross-linked EOC networks (EOCXs) and dynamically cross-linked EOC CANs, the latter of which contain BTMA cross-linker that endows them with dissociative dialkylamino disulfide dynamic chemistry,[85-88] from EOCs of varying 1-

octene content and MFI. In doing so, we confirm that increasing 1-octene content and MFI in precursor EOCs generally decreases cross-link density in EOCXs. For the first time, we report that EOC CANs exhibit 1-octene and MFI trends similar to EOCXs: as 1-octene content and MFI increase in precursor EOCs, cross-link density decreases in EOC CANs. Evidenced by temperature-dependent storage moduli (*E'*) in EOC CANs, we demonstrate the dissociative nature of the dialkylamino disulfide dynamic chemistry and that EOC CANs of lower cross-link density exhibit steeper declines in *E'* with increasing temperature, corresponding to a more severe loss of network architecture. As opposed to EOCXs, our EOC CANs are fully reprocessable and completely recover their cross-link densities and associated properties after two reprocessing cycles. We also address stress relaxation of our EOC CANs. We confirm that decreasing cross-link density in EOC CANs generally leads to shorter average stress relaxation times across a wide temperature range and that the stress relaxation responses of the CANs are largely dominated by dialkylamino disulfide dynamic chemistry.

## 2. Experimental

**2.1. Materials.** All chemicals were used as received unless otherwise stated. 2,2,6,6-tetramethyl-4-piperidyl methacrylate (TMPM) was purchased from TCI America. Petroleum ether (anhydrous), sulfur monochloride ($S_2Cl_2$, 98%), *o*-xylene (98%), and dicumyl peroxide (DCP, 98%) were purchased from Sigma-Aldrich. All ethylene/1-octene copolymers ($Đ$ ~ 2-3)[124] and propylene/ethylene copolymer samples were received from The Dow Chemical Company. 1-Octene contents and molecular weight information of the EOCs were provided by the supplier, as were the MFIs (I2), as measured by ASTM D-1238 at 190 °C and 2.16 kg. Petroleum ether was dried over activated 4 Å molecular sieves for at least 48 h before use. After its initial use as received, $S_2Cl_2$ was distilled and dried over activated 4 Å molecular sieves for at least 48 h before further use.

**2.2. Synthesis of BiTEMPS Methacrylate (BTMA) Cross-Linker.** Unless stated otherwise, bis(2,2,6,6-tetramethyl-4-piperidyl methacrylate) disulfide (BiTEMPS methacrylate, BTMA) was

synthesized, purified, and characterized according to literature procedures.[85,87] 2,2,6,6-tetramethyl-4-piperidyl methacrylate (TMPM) (~8.78 g, 39.0 mmol) was dissolved in ~100 mL of dry petroleum ether and cooled to −70 °C in a dry ice/acetone bath. Subsequently, $S_2Cl_2$ (~1.3 g, 9.7 mmol) was dissolved in ~1.25 mL of dry petroleum ether, and this solution was added dropwise to TMPM while stirring. After addition, the solution was stirred for 15 min at −70 °C and for 30 min at room temperature. The contents of the reaction vessel were washed in distilled water, precipitating creamy, off-white solid chunks. After vacuum filtering and oven drying the crude product at 50 °C for 48 h, BTMA was obtained (~2.4 g).[85,87] See the Supporting Information for the synthesis procedure of BTMA for reprocessing studies via extrusion.

BTMA syntheses result in the formation of polysulfide derivatives of BTMA such as trisulfides and tetrasulfides as minor products.[83,88,125] We acknowledge that these polysulfide derivatives may be present in small amounts in our BTMA cross-linker even after rigorous organic workup. Freshly distilling $S_2Cl_2$ prior to BTMA synthesis and completing the synthesis in an inert environment limit the formation of polysulfides. Column chromatography may be used to isolate the BTMA synthesis product with the desired bridge length.[83,125] Polysulfide analogues of BiTEMPS-based cross-linkers have been shown previously to have dynamic character similar to disulfide analogues of BiTEMPS-based cross-linkers.[125] Any polysulfides present in our BTMA cross-linker have negligible effects on the thermomechanical properties and reprocessability of our EOC CANs indicated by the results present in the following sections.

**2.3. Synthesis of EOC CANs and Permanently Cross-linked EOCs (EOCXs).** To obtain EOC CANs, EOC pellets (1.0 to 2.0 g basis) were added to an Atlas Laboratory Mixing Molder (flushed twice with respective EOC before synthesis) with crushed powders of BTMA (5 wt%), DCP (1 wt%), and three steel balls to emulate the chaotic mixing of reactive extrusion.[126] The wt%s of BTMA and DCP were calculated relative to the mass of the EOC added to the mixer. All EOC/BTMA/DCP blends were melt-state homogenized at 100 °C and 120 RPM for 3-5 min. The rotor was cycled up and down manually to aid in mixing. After, the uncured blends were removed from the mixer by spatula and compression molded in a PHI press (Model 0230C-X1) at 180 °C

with a 10-ton ram force (~8 MPa) for 30 min. This compression molding step serves to cross-link the blends and produce 1st-molded EOC CAN sample films (~0.6-mm thick). EOCX sample films were synthesized with 1 wt% DCP by the same procedure without BTMA.

**2.4. Reprocessing of EOC CANs via Compression Molding.** 1st-molded EOC CANs were cut into millimeter-sized pieces and compression molded at 180 °C with a 10-ton ram force (~8 MPa) for 5 min into 2nd-molded sample films. Similarly, 2nd-molded EOC CANs were cut into pieces and compression molded at the same conditions into 3rd-molded sample films. EOCXs were unable to be reprocessed from 1st-molded films into healed 2nd-molded films at the same compression molding conditions.

**2.5. Rheological Curing Study.** Curing studies of EOCXs and EOC CANs were performed via small-amplitude oscillatory shear (SAOS) measurements at 180 °C using an Anton-Paar MCR 302 rheometer with an oven hood attachment and a 25-mm parallel plate fixture. Uncured sample discs ~2 mm in thickness were prepared by compression molding uncured blends from the melt mixer at 100 °C with a 10-ton ram force (~8 MPa). An oscillatory shear strain of 0.1% was applied to each disc at a 1 Hz frequency at 180 °C with 0 N of normal force. Shear storage moduli ($G'$) were monitored as functions of time and used to indicate the extent of cross-linking in the samples.

**2.6. Gel Content Determination.** EOC CANs and EOCXs were cured by compression molding at 180 °C with a 10-ton ram force (~8 MPa) for 30 min into discs ~2 mm in thickness and ~23 mm in diameter. Discs were massed ($m_d$, typically 0.6 g), placed into Growing Labs cellulose Soxhlet extraction thimbles, and immersed in boiling *o*-xylene under reflux at 165 °C for 12 h. The insoluble network fractions were vacuum dried for 48 h and massed ($m_o$). Gel contents were determined as follows: gel content % = 100 ($m_o/m_d$).

**2.7. Fourier Transform Infrared (FTIR) Spectroscopy.** Room-temperature attenuated total reflectance-Fourier transform infrared (ATR-FTIR) spectroscopy was conducted using a Bruker Tensor 37 MiD FTIR spectrophotometer equipped with a diamond/ZnSe ATR attachment. For each sample, sixteen scans were collected over a 4000 to 600 $cm^{-1}$ range at 4 $cm^{-1}$ resolution.

**2.8. Grafting Efficiency Determination.** The grafting efficiencies of EOC CANs were

determined using FTIR calibration curves. Physical mixtures of each EOC and varying amounts (1 to 7 wt%) of BTMA were prepared by melt-mixing at 100 °C. The mixtures were characterized by FTIR spectroscopy to generate calibration curves of BTMA carbonyl peak intensity (~1720 $cm^{-1}$) normalized by C−H peak intensity (1470 $cm^{-1}$) as a function of BTMA wt%.

For a typical grafting efficiency determination, ~100 mg of an EOC CAN sample were added to a 20-mL glass scintillation vial containing ~25 mg BTMA (~500% in excess relative to the BTMA added to CANs during EOC CAN synthesis) dissolved in 5 mL *o*-xylene. Excess BTMA served to decross-link the CAN after BTMA cross-links undergo exchange reactions with ungrafted BTMA molecules. The mixture was kept at 120 °C with stirring overnight to melt and decross-link the EOC CAN. Decross-linking caused the CAN to dissolve, and a clear solution was obtained; the decross-linked EOC was collected by precipitation in 200 mL acetone and dried. After, the decross-linked EOC was characterized by FTIR spectroscopy. The grafting efficiency was obtained as follows: 100 $(wt\%)_{decross}/(wt\%)_{CAN}$, where $(wt\%)_{decross}$ refers to the BTMA wt% in the decross-linked EOC obtained from the corresponding EOC CAN FTIR calibration curve, and $(wt\%)_{CAN}$ refers to the wt% BTMA in as-synthesized EOC CANs (5 wt%).

**2.9. Differential Scanning Calorimetry (DSC).** A Mettler Toledo DSC822e was used to conduct DSC experiments on ~5-mg samples of EOCs, EOC CANs, and EOCXs in hermetically sealed aluminum pans under nitrogen flow. The following temperature cycle was applied to samples during testing: samples were heated to 180 °C at a rate of 10 °C/min, held at 180 °C for 5 min, and cooled to –40 °C at the same rate. This heating and cooling cycle was repeated, completing a second scan. From the second heating and cooling scans, relevant melting and crystallization peak temperatures were determined from the endothermic and exothermic peaks, respectively. Melting endpoint and crystallization onset temperatures were similarly determined from the respective peaks of the second scan. Percent crystallinities were determined by integrating crystallization peaks to obtain latent heats of fusion of samples and calculating the ratio of these latent heats against the latent heat of fusion for fully crystalline PE of 293 J/g.[2,127]

**2.10. Dynamic Mechanical Analysis (DMA).** Tension-mode DMA experiments were conducted

on rectangular-cut samples using a TA Instruments RSA-G2 Solids Analyzer. For temperature-ramp experiments, storage modulus (*E'*), loss modulus (*E''*), and damping ratio ($\tan\delta = E''/E'$) were measured as functions of temperature at a heating rate of 3 °C/min with 1.0 Hz frequency and 0.03% oscillatory strain under air flow. For frequency-sweep experiments, *E'* was measured within a frequency range of 0.01 Hz to 100 Hz with 0.03% oscillatory strain at 100 °C.

**2.11. Tensile Testing.** Room-temperature tensile properties of EOCs, EOCXs, and (re)processed EOC CANs were characterized using an MTS Criterion Electromechanical Test System. Dog-bone-shaped samples with 4.7 mm x 0.7 mm x 22 mm dimensions were cut from compression-molded films using a Dewes-Gumbs die. Samples were pulled by the tensile tester at an extension rate of 130 mm/min, and 350 data points were collected per second until samples broke. Tensile strengths are reported as the maximum stress values in the resulting stress-strain curves. Young's moduli are calculated from $E = \Delta\sigma/\Delta\varepsilon$, where $\Delta\sigma$ and $\Delta\varepsilon$ are the respective changes in stress and strain in the linear elastic region of the stress-strain curves in the limit of zero strain. Elongations at break are reported as the % strains at sample breakages.

**2.12. Creep.** Tensile creep experiments were conducted by hanging a 0.33 MPa load on molded dog-bone-shaped samples (4.7 mm x 0.7 mm x 22 mm dimensions) in an oven at 50 °C. Sample lengths were measured periodically with a caliper, and % strains were calculated from these lengths relative to the initial sample lengths after loading as follows: 100 (final length – initial length)/initial length.

Shear creep experiments were conducted with a 3.0 kPa stress on molded disc samples (2 mm in thickness, 23 mm in diameter) using an Anton-Paar MCR 302 rheometer and a 25-mm parallel plate fixture. Samples were equilibrated at 90 °C for 10 min before commencing experiments. 10 N of normal force were used. Creep tests were carried out for 10000 s. Viscous creep strains were calculated by extrapolating lines fitted between $t$ = 9000 and $t$ = 10000 s to $t$ = 0 s and subtracting these y-intercepts from the corresponding final strain values at $t$ = 10000 s.

**2.13. Stress Relaxation.** Tension-mode stress relaxation experiments were conducted on rectangular-cut 1$^{st}$-molded EOC CANs using a TA Instruments RSA-G2 Solids Analyzer. Testing

temperatures were 100 °C, 120 °C, 140 °C, and 160 °C. Samples were thermally equilibrated at the testing temperature for 10 min before commencing tests. An instantaneous, constant 3% strain was applied during testing. Stress relaxation modulus ($E$(t)) for each sample was monitored as a function of time until it had relaxed at least 80% of its initial value.

**2.14. Reprocessing of CANs via Extrusion.** Proof-of-concept extrusion was conducted in an Xplore MC 40 micro compounder. EOC CAN-38-1 was prepared with 5 wt% BTMA and 1 wt% DCP and cured via compression molding at 180 °C for 15 min and 40000 psi. The CAN was cut into pieces, and 15-20 g were fed into the hopper of the micro compounder. The CAN was circulated through the screws for 5 min at 200 °C and 25 rpm, after which it was extruded.

## 3. Results and Discussion

**3.1. Synthesis of Permanently Cross-linked EOCs (EOCXs) and Dynamically Cross-linked EOCs (EOC CANs).** We synthesized permanently cross-linked EOC networks (EOCXs) and dynamically cross-linked EOC CANs from a collection of random ethylene/1-octene copolymers (EOCs) with varying 1-octene contents and MFIs. Table 1 summarizes the properties of the random EOCs.[124] The EOCs are referred to using the naming convention: EOC-*x*-*y*, where *x* is 1-octene wt% and *y* is MFI (e.g., EOC-30-1 indicates the EOC with 30 wt% 1-octene comonomer and an MFI of 1). Prior to EOCX and EOC CAN syntheses, neat EOCs were characterized using differential scanning calorimetry; thermal properties from DSC are given in Table S1. With increasing 1-octene content, neat EOCs exhibit decreasing crystallinities as well as melt transitions at lower temperatures. EOC-30-1, the EOC with the lowest 1-octene content, exhibits the largest crystallinity of 23% and peak melting temperature ($T_{m,peak}$) of 81 °C. EOC-45-1, the EOC with the highest 1-octene content, exhibits the lowest crystallinity of 11% and $T_{m,peak}$ of 50 °C. As 1-octene content increases, the fraction of crystallizable ethylene in the corresponding EOC decreases, leading to the formation of thinner crystals. Also, the short chain branches provided by greater 1-octene contents enhance the segmental mobility of adjacent crystallizable regions. These factors cause the lower crystallinities and melting transitions as 1-octene content increases in EOCs.

**Table 1.** Neat EOC property information.

| Material | 1-Octene Content (wt%)[a] | Melt Flow Index (g/10 min)[a] | $M_w$ (g/mol)[a] | Density (g/cm$^3$)[a] | Crystallinity (%)[b] |
|---|---|---|---|---|---|
| **EOC-30-1** | 30 | 1 | 80,000-130,000 | 0.885 | 23 |
| **EOC-38-1** | 38 | 1 | 80,000-130,000 | 0.870 | 18 |
| **EOC-45-1** | 45 | 1 | 100,000-150,000 | 0.857 | 11 |
| **EOC-38-5** | 38 | 5 | 60,000-90,000 | 0.870 | 19 |
| **EOC-31-30** | 31 | 30 | 30,000-60,000 | 0.885 | 15 |

[a]Data provided by manufacturer.[124] [b]Determined by DSC. Listed values are ± 1%.

From the neat EOCs, EOCX and EOC CAN samples were synthesized using dicumyl peroxide (DCP) as the radical initiator and, in the case of the EOC CANs, BiTEMPS methacrylate (BTMA) as the pre-synthesized, dynamic cross-linker. At temperatures above 80 °C, the disulfide bond in BTMA undergoes homolytic dissociation into stable sulfur-centered radicals which do not react readily with oxygen, olefins, phosphites, and other molecular substrates that react readily with free radicals.[83-85,128-130] Below 80 °C, these sulfur-centered radicals recombine with one another.[83,84,128,131] This reversible dissociation allows CANs synthesized with BTMA cross-links to be reprocessed at high temperature.[83-85,87,88] To synthesize our EOCXs and EOC CANs, we modified our procedure from ref. 88 in which we synthesized PE CANs via dynamically cross-linking PE with BTMA and DCP at 160 °C by melt-mixing for 30 min and compression molding for 30 min. Here, we instead melt-mixed EOC/DCP and EOC/BTMA/DCP blends at 100 °C and 120 RPM for 3-5 min before removing these uncured blends and compression molding them at 180 °C for 30 min. By melt-state homogenizing at 100 °C, we avoided initiating the DCP prematurely, and the compression molding step at 180 °C serves to cross-link the EOC/DCP and EOC/BTMA/DCP blends into EOCXs and EOC CANs, respectively. From our previous study synthesizing PE CANs by a similar procedure with BTMA and DCP, we found that loadings of 5 wt% BTMA and 1 wt% DCP each with respect to the mass of PE led to robustly cross-linked and reprocessable PE CANs.[88] Thus, we chose to maintain that formulation to prepare EOC CANs for

the entirety of this study unless otherwise specified. Accordingly, all EOC CANs were cross-linked with 5 wt% BTMA and 1 wt% DCP, and all EOCXs were cross-linked with only 1 wt% DCP.

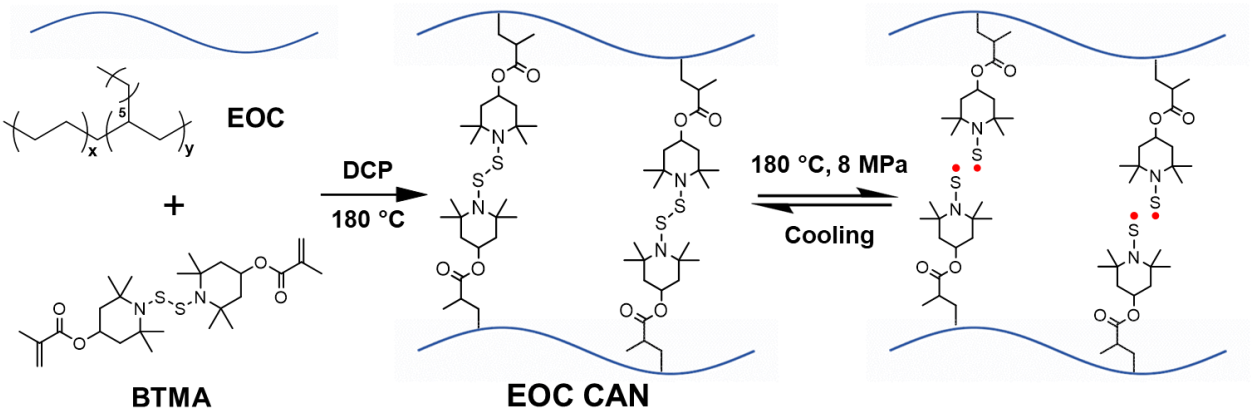


**Figure 1.** Synthesis of ideal EOC CAN from a representative EOC, BiTEMPS methacrylate (BTMA), and dicumyl peroxide (DCP) at compression molding conditions. BTMA cross-links dissociate at reprocessing conditions into stable sulfur-centered radicals that reform cross-links upon cooling. An EOC CAN may also feature runs of BTMA units as cross-links as well as small amounts of loops or permanent cross-links. See Figure S1 for these possible chemistries.

During the cross-linking of EOCs, the peroxide bond in DCP dissociates to form two free radicals at 180 °C. These free radicals may extract hydrogen atoms from the EOC backbone to form carbon macroradicals. Permanent cross-links are formed when two carbon macroradicals terminate by combination. In EOC CANs, the carbon macroradicals may react with the carbon-carbon double bonds in BTMA. When one of the two carbon-carbon double bonds in BTMA is attacked by a carbon macroradical, a BTMA graft is formed on an EOC backbone chain. Following an initial graft, propagation of a radical through BTMA may occur to form runs of more than one BTMA unit as grafts. When the second carbon-carbon double bond on a grafted BTMA unit or run of BTMA units is grafted to a separate EOC backbone chain, a dynamic cross-link is formed.[88] Figure 1 depicts the synthesis of an ideal EOC CAN from an EOC, BTMA, and DCP as well as the dynamic chemistry of the BTMA cross-links. Other chemistries are possible in small amounts

when preparing EOC CANs such as loop formation, dangling BTMA grafts, or permanent cross-linking (Figure S1). As demonstrated further below, by incorporating 5 wt% BTMA alongside 1 wt% DCP, a sufficient number of dynamic BTMA cross-links are formed, and the level of permanent cross-links is maintained below a percolation threshold. As such, we may reprocess our EOC CANs into fully healed films.

As described above, EOCXs and EOC CANs were obtained after compression molding their uncured, precursor blends at 180 °C for 30 min. We determined 30 min to be the necessary cross-linking time by conducting isothermal curing studies on uncured blends at 180 °C. Prior to curing studies, we processed uncured EOC/DCP and EOC/BTMA/DCP blends out of the melt-mixer into discs (~ 2 mm thickness, ~25 mm diameter) by compression molding at 100 °C. Small-amplitude oscillatory shear (SAOS) experiments were conducted on each disc in which a 0.1% oscillatory strain was applied at a frequency of 1.0 Hz at 180 °C. Curing was monitored by shear storage modulus (*G*') measurements as a function of time, and the results for each EOCX and EOC CAN are plotted in Figure S2. As time elapses, the normalized *G*' of each sample increases, indicating an increase in the elastic character, and therefore cross-link density, of each. The $t_{95}$ values, which indicate the respective times when *G*' reaches 95% of its maximum value, were noted for EOCXs and EOC CANs; these data are presented in Table S2. All EOCXs and EOC CANs exhibit $t_{95}$ values between 20 and 30 min at 180 °C, indicating that a reactive processing step by compression molding at this temperature for 30 min will sufficiently cross-link all EOC samples. Based on these tests, we standardized 30 min as our compression molding time for cross-linking in our procedure. We note that, on average, EOCXs exhibit slightly shorter $t_{95}$ values relative to EOC CANs, suggesting that dynamic cross-linking of EOCs with BTMA must proceed for slightly longer times in order to approach their maximum cross-linking levels relative to their EOCX counterparts.

We confirmed the presence of BTMA as a grafted cross-linker in our EOC CANs by FTIR spectroscopy. The methacrylate carbonyl in BTMA exhibits a stretching peak around 1720 $cm^{-1}$ in the FTIR spectra of EOC CANs;[88] see Figure S3 for the FTIR spectra of EOC-38-1, EOCX-38-1, and EOC CAN-38-1 as examples. The BTMA carbonyl peak is present in the FTIR spectra of

EOC CAN-38-1 samples before and after Soxhlet extraction in boiling *o*-xylene to remove sol fractions. This indicates that BTMA was successfully grafted to EOC chains, as any BTMA left ungrafted on both methacrylates, and therefore inertly dispersed in the EOC matrix, would have washed away during Soxhlet extraction. As expected, the BTMA carbonyl peak is not present in the spectra of neat or permanently cross-linked EOCs.

We quantified the grafting efficiencies during EOC CAN syntheses using FTIR spectroscopy calibration curves obtained from physical mixtures of each EOC and varying wt%s of BTMA. (See Figures S4-S7.) The as-synthesized EOC CANs were melted and decross-linked in *o*-xylene with excess BTMA; the decross-linked EOCs were precipitated in acetone. (See additional details in the Experimental section.) The wt% of grafted BTMA in the decross-linked EOCs was determined using the respective FTIR calibration curves, and the grafting efficiency, which refers to the percentage of BTMA successfully grafted in the gel fraction of the EOC CAN relative to BTMA added during EOC CAN synthesis, was quantified. As shown in Table 2, EOC CAN-30-1 exhibits the highest grafting efficiency of the EOC CANs. This is likely the result of EOC-30-1 having the lowest 1-octene content of the precursor EOCs, meaning it contains longer backbone ethylene sequences for BTMA grafting. For EOC CANs with an MFI of 1, as 1-octene content increases, grafting efficiency expectedly decreases. As described further below, these differences in grafting efficiency have implications on the thermomechanical properties of the EOC CANs. Increasing MFI in EOCs of constant 1-octene content also decreases average BTMA grafting efficiency (52 ± 3% for EOC CAN-38-1 vs. 43 ± 5% for EOC CAN-38-5), likely a result of the shorter chains present in the precursor EOC-38-5 relative to EOC-38-1 that are available for BTMA grafting.

**3.2. Effects of 1-Octene Content and MFI on EOCX and EOC CAN Properties.** By incorporating this 30-min compression molding step into our procedure, we obtained 1$^{st}$-molded EOCX and EOC CAN films. The thermomechanical properties of 1$^{st}$-molded EOCX and EOC CAN samples were characterized by temperature-ramp dynamic mechanical analyses (DMA);

**Table 2.** BTMA grafting efficiencies of EOC CANs and gel contents of EOCXs and EOC CANs.

| Sample | BTMA Grafting Efficiency (%) | Gel Content (%) |
|---|---|---|
| EOCX-30-1 | - | 88 ± 3 |
| EOCX-38-1 | - | 89 ± 1 |
| EOCX-45-1 | - | 88 ± 1 |
| EOCX-38-5 | - | 80 ± 2 |
| EOC CAN-30-1 | 64 ± 3 | 67 ± 9 |
| EOC CAN-38-1 | 52 ± 3 | 64 ± 6 |
| EOC CAN-45-1 | 39 ± 5 | 58 ± 6 |
| EOC CAN-38-5 | 43 ± 5 | 18 ± 7 |

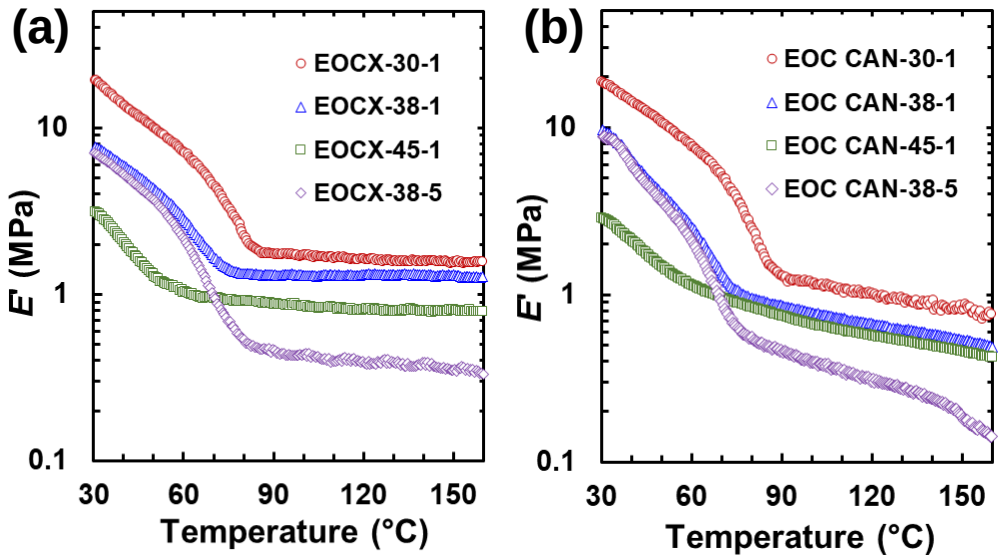


**Figure 2.** Tensile storage modulus (*E'*) as a function of temperature for 1st-molded (a) EOCXs and (b) EOC CANs.

these data are in Figure 2 and Table S3. As shown by the storage modulus (*E'*) curves plotted in Figure 2, all 1st-molded EOCX and EOC CAN samples exhibit melt transitions some tens of degrees above 30 °C followed by quasi-rubbery plateaus up to 160 °C. The presence of these rubbery plateaus indicates the cross-linked nature of the EOCXs and EOC CANs, as their neat EOC precursors flow above their melt transitions and do not exhibit rubbery plateaus of these magnitudes (DMA curves for neat EOCs are shown in Section 3.4.). Flory's ideal rubber elasticity theory states that tensile modulus, *E*, is linearly proportional to effective cross-link density and

absolute temperature.[132] In the rubbery plateaus of the cross-linked networks, *E'* is vastly larger than *E"*, so we may approximate *E* using *E'* in this regime. Thus, the cross-link densities of EOCXs and EOC CANs were assessed using their *E'* rubbery plateaus by DMA.

In general, EOC CANs exhibit lower cross-link densities than their respective EOCX counterparts as evidenced by lower *E'* rubbery plateaus (Figure 2 and Table S3). This may be due to the formation of longer runs of BTMA units as cross-links or intra-chain loops during dynamic cross-linking to produce EOC CANs with reduced cross-link densities. EOC CANs and EOCXs also differ in the temperature dependences of their *E'* rubbery plateaus. It is evident that each EOC CAN exhibits a declining *E'* rubbery plateau with increasing temperature (hence, the use of the term "quasi-rubbery plateau"). This decreasing *E'* rubbery plateau behavior with increasing temperature is indicative of the dissociative nature of the BTMA dynamic chemistry in the EOC CANs.[85,87,88] In contrast, the *E'* rubbery plateau of an ideal, cross-linked rubber will exhibit a linear increase with increasing temperature.[132] As demonstrated in previous work involving dialkylamino disulfide dynamic chemistry, CANs endowed with BTMA units as dynamic cross-links will exhibit a decreasing temperature-dependent *E'* rubbery plateau reflecting the greater number of dissociating cross-links (and therefore decreasing cross-link density) as temperature increases.[85,87,88]

For 1$^{st}$-molded EOCXs and EOC CANs with a constant MFI of 1, *E'* rubbery plateaus at all temperatures generally decrease as 1-octene content increases. For EOCXs and EOC CANs, respectively, EOCX-30-1 and EOC CAN-30-1 exhibit the highest average *E'* rubbery plateaus, followed by EOCX-38-1/EOC CAN-38-1, then EOCX-45-1/EOC CAN-45-1. The 1$^{st}$-molded EOC CAN-38-1 and 1$^{st}$-molded EOC CAN-45-1 exhibit *E'* quasi-rubbery plateaus that are within experimental error of one another at all temperatures (0.48 ± 0.03 MPa and 0.44 ± 0.05 MPa at 160 °C, respectively). Therefore, at some 1-octene content between 30 and 38 wt%, there appears to be no further significant decrease in cross-link density with increasing 1-octene content via dynamic cross-linking with BTMA.

For 1st-molded EOCXs and EOC CANs with constant 1-octene contents, we observed that *E'* rubbery plateaus at all temperatures decrease as MFI increases. As evidenced by DMA data in Figure 2 and Table S3, EOCX-38-1 and EOC CAN-38-1 exhibit greater *E'* rubbery plateaus than their respective counterparts, EOCX-38-5 and EOC CAN-38-5, at all temperatures. It is worth noting that we attempted to cross-link EOC-31-30 dynamically into EOC CAN-31-30 to compare to EOC CAN-30-1. The resulting EOC CAN-31-30 exhibited a very weak quasi-rubbery plateau above its melt transition at very low *E'* relative to EOC CAN-30-1 (Figure S8(a)). This low *E'* quasi-rubbery plateau suggests that attempting to cross-link EOC-31-30 likely resulted in increased branching and very light cross-linking of chains. Efforts to cross-link EOC-31-30 using 10 wt% BTMA and 2 wt% DCP still led to a significantly reduced *E'* rubbery plateau compared to EOC CAN-30-1 (Figure S8(b)). As a result, we discontinued studies using EOC-31-30, including attempting to synthesize EOCX-31-30.

The effect of frequency on the rubbery-state *E'* plateaus of the EOCXs and EOC CANs was studied by frequency-sweep DMA measurements at 100 °C. As shown in Figure S9, all EOC CANs show larger frequency dependence of *E'* compared to their EOCX counterparts. Previous studies have demonstrated that the dialkylamino disulfide bonds are dynamic at temperatures as low as 80 °C.[87] Therefore, these observations of larger frequency dependence in EOC CANs indicate that dynamic bond exchange at high temperatures partially contributes to their lower *E'* rubbery plateaus relative to EOCXs.

We determined gel contents on 1st-molded EOCXs and EOC CANs, and these data are present in Table 2. This was done via Soxhlet extraction to remove the sol fractions of the gelled networks for 36 h in boiling *o*-xylene before vacuum drying for 48 h. All EOCXs exhibited greater gel contents than their respective EOC CANs derived from the same precursor EOC. Gel contents for 1st-molded EOCXs with an MFI of 1 are within experimental uncertainty of one another; this is also the case for 1st-molded EOC CANs with an MFI of 1 (despite their average gel contents decreasing as 1-octene increases). Thus, the differences in the cross-link densities of these EOCXs

and EOC CANs of increasing 1-octene content evidenced by rubbery plateau *E'* data are not strongly reflected by differences in their gel contents.

We also found that the gel contents of EOCXs and EOC CANs of the same 1-octene content decrease as MFI increases. EOCX-38-1 and EOC CAN-38-1 each have greater gel contents (89 ± 1% and 64 ± 6%, respectively) than their constant 1-octene analogues with an MFI of 5, EOCX-38-5 and EOC CAN-38-5 (80 ± 2% and 18 ± 7%, respectively). These results corroborate the respective lower cross-link densities of EOCX-38-5 and EOC CAN-38-5 relative to EOCX-38-1 and EOC CAN-38-1. In the case of EOCX-38-1 and EOCX-38-5, their 9% difference in gel content also further suggests that decreasing cross-link density resulting in a significant reduction in *E'* rubbery plateau (over a three-fold decrease from EOCX-38-1 to EOCX-38-5 at 160 °C) does not have as strong of an effect on gel content for EOCXs.

In total, the observations from EOCXs and EOC CANs show that with higher 1-octene content in precursor EOCs, *E'* rubbery plateaus and cross-link densities in the resulting cross-linked samples decrease. Increasing 1-octene content in EOCs increases the number of sterically hindering branches that may inhibit macroradical formation from the bulky initiator and interactions between macroradicals and BTMA.[37,133] Increasing 1-octene content in EOCs also increases the number of tertiary carbons that are vulnerable to β-scission over cross-linking in the presence of radical species.[17,37,48,133] These factors decrease the propensity for EOCs with higher 1-octene content to cross-link into EOCXs and EOC CANs compared to EOCs with lower 1-octene content. It is also evident that increasing MFI in EOCs decreases their propensities to cross-link as well as the resulting cross-link density of the EOCX and EOC CAN sample. Increased MFI in EOCs reflects decreased weight-average molecular weight ($M_w$), resulting in a greater number of chain ends that are unable to cross-link as well as the need for more cross-links between chains in order to obtain a sufficiently percolated network architecture.[41,133]

To explore our previous point about greater numbers of tertiary carbons in polymers negatively influencing their cross-linkability, we conducted a control experiment in which we attempted to dynamically cross-link a propylene/ethylene copolymer (PEC) with 79 wt%

propylene content. It was hypothesized that 79 wt% propylene in this PEC would provide a sufficient number of tertiary carbons to promote chain scission and molecular-weight reduction over cross-linking in the presence of DCP.[134,135] After a cross-linking attempt of the PEC with 5 wt% BTMA and 1 wt% DCP, the resulting PEC CAN exhibited a significantly reduced semicrystalline *E'* relative to its PEC precursor. (See Figure S10.) The PEC CAN also displayed a steep and continuously decreasing *E'* above its melt transition, and the absence of even a quasi-rubbery plateau at these temperatures indicates little to no percolated network structure in the PEC after the cross-linking attempt. These features imply that β-scission was more prominent than cross-linking during our attempt, leading to molecular-weight reduction of the PEC.[134,136] This observation strongly supports that a greater presence of tertiary carbons in a polymer will negatively impact its cross-linkability through increased β-scission.

We quantified the loss of *E'* in the rubbery plateau of each EOC CAN with increasing temperature by plotting normalized *E'* (*E'*(*T*) relative to *E'* at 100 °C) as a function of temperature; see Figure 3. We observe that EOC CAN-30-1, the EOC CAN with the largest cross-link density, exhibits the smallest decrease in normalized *E'*, indicating that it lost the least amount of cross-link density with increasing temperature. Steeper declines are evident for EOC CAN-38-1 and EOC CAN-45-1 (nearly identical) with the steepest decline in normalized *E'* exhibited by EOC CAN-38-5, the EOC CAN with the smallest cross-link density. Thus, we observe that lower cross-link density in EOC CANs generally correlates with greater decreases in normalized *E'*, and therefore cross-link density, with increasing temperature because of the dissociating BTMA cross-links. As all EOC CANs have BTMA dynamic cross-links with similar temperature dependences of dissociation,[83,87,88,125] we interpret that this correlation reflects that the loss of a very small fraction of cross-links in a loose or barely percolated polymer network (e.g., EOC CAN-38-5) will lead to a substantial loss of percolation of the cross-links. Cross-links that do not percolate across the material do not contribute significantly to the *E'* rubbery plateau, resulting in a more severe *E'* reduction with increasing temperature. Accordingly, EOC CANs with larger percolated cross-link

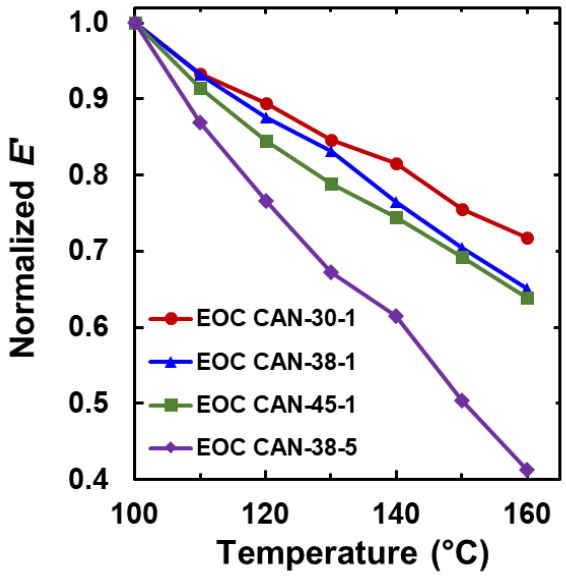


**Figure 3.** Normalized *E*' (*E'*(*T*) relative to *E*' at 100 °C) as a function of temperature in the rubbery plateau regimes of EOC CANs.

densities (lower 1-octene content and MFI in precursor EOC, e.g., EOC CAN-30-1) are expected to exhibit smaller losses of percolated cross-link density with increasing temperature.

Mechanical properties of EOCs, EOCXs, and EOC CANs were also evaluated by tensile tests at room temperature (Figure S11 and Table 3). Generally, Young's moduli (*E*) of 1$^{st}$-molded EOC CANs were comparable (within experimental uncertainty) to their precursor EOC and EOCX counterparts. After permanent and dynamic cross-linking, average tensile strengths and elongations at break of EOCs generally decreased or remained within experimental uncertainty of their respective cross-linked EOCXs and EOC CANs. These behaviors are characteristic of semi-crystalline, cross-linked materials synthesized from semi-crystalline thermoplastics. Room-temperature tensile properties were expected to decrease slightly due to the decreases in crystallinity when cross-linking EOCs into EOCXs and EOC CANs; in some cases, the introduction of cross-links partially made up for tensile property losses caused by crystallinity reductions. EOCXs generally exhibited lower yet comparable elongations at break and tensile strengths to their EOC CAN counterparts. For EOCXs and EOC CANs with a constant MFI of 1,

*E* values and tensile strengths generally decrease on average and elongations at break generally increase on average as 1-octene content increases, trends expected based on those for precursors EOCs with 1-octene content. When comparing EOCXs with a constant 1-octene content of 38 wt%, *E* values and tensile strengths decrease and elongations at break increase with increasing MFI. Interestingly, EOC CAN-38-5 exhibits a lower tensile strength than but comparable *E* and elongation at break to those of EOC CAN-38-1 despite the increased MFI of the precursor EOC used to make EOC CAN-38-5.

**Table 3.** Room-temperature tensile properties of EOCs, EOCXs, and EOC CANs.

| Material | Sample | Young's modulus (MPa)[a] | Tensile strength (MPa)[a] | Elongation at break (%)[a] |
|---|---|---|---|---|
| **EOC-30-1** | Neat | 19.4 ± 3.5 | 19.3 ± 1.1 | 720 ± 15 |
| | EOCX-30-1 | 19.6 ± 5.7 | 12.6 ± 2.7 | 610 ± 20 |
| | EOC CAN-30-1 | 21.7 ± 1.1 | 13.4 ± 2.1 | 650 ± 70 |
| **EOC-38-1** | Neat | 9.1 ± 1.3 | 12.9 ± 0.9 | 800 ± 40 |
| | EOCX-38-1 | 9.7 ± 0.8 | 11.3 ± 0.2 | 620 ± 30 |
| | EOC CAN-38-1 | 7.6 ± 3.5 | 14.9 ± 1.9 | 700 ± 110 |
| **EOC-45-1** | Neat | 3.9 ± 0.6 | 6.4 ± 1.1 | 1060 ± 60 |
| | EOCX-45-1 | 3.7 ± 0.4 | 3.8 ± 0.8 | 610 ± 90 |
| | EOC CAN-45-1 | 3.0 ± 0.1 | 5.1 ± 1.2 | 830 ± 120 |
| **EOC-38-5** | Neat | 8.0 ± 0.1 | 11.9 ± 2.0 | 1100 ± 160 |
| | EOCX-38-5 | 9.7 ± 0.1 | 6.9 ± 1.5 | 600 ± 60 |
| | EOC CAN-38-5 | 7.8 ± 0.9 | 8.7 ± 1.2 | 760 ± 80 |

[a]Determined by tensile testing. Error bars represent ± one standard deviation of three measurements.

We also conducted creep experiments on an EOC CAN and its precursor EOC to demonstrate the added creep resistance after dynamic cross-linking. We subjected EOC CAN-45-1 to two sets of conditions for creep testing: (1) tensile load of 0.33 MPa at 50 °C for 48 h and (2) shear load of 3.0 kPa at 90 °C for 10000 s. After creep testing with set 1, EOC CAN-45-1 exhibited 84 ± 4% strain after 2.5 h (Figure S12); one sample exhibited 116% strain after 48 h. EOC-45-1 samples broke within 1 min at 50 °C after the application of the 0.33 MPa load. We also observed that dynamic cross-linking endows EOC CAN-45-1 with considerable creep resistance relative to EOC-45-1 in its rubbery state at the set 2 conditions. After 10000 s, EOC CAN-45-1 accumulated 9.2% viscous creep strain, whereas the molten EOC-45-1 had strained 3300% after only 2500 s

(Figure S13). These results demonstrate the substantial improvement in creep resistance in both the semi-crystalline and molten states of the EOCs after dynamically cross-linking EOC-45-1 into EOC CAN-45-1.

**3.3. Stress Relaxation of EOC CANs.** To assess the temperature dependence of the dynamic BTMA cross-link dissociation across EOC CANs, we conducted stress relaxation experiments on 1st-molded EOC CAN samples at several temperatures. 1st-molded EOC CANs were subjected to a 3% strain, a sufficiently small strain such that the responses of the EOC CANs are in their linear viscoelastic regimes, and the stress relaxation moduli were monitored as a function of time. Figure 4 displays the normalized stress relaxation modulus ($E$(t)/$E_0$) vs. time data for EOC CANs. We then fitted these data to the Kohlrausch-Williams-Watts (KWW) stretched exponential decay function (Eqn. 1) to account for the breadth of relaxation times experienced by the polymers.[137-139] This function is expressed as follows:

$$\frac{E(t)}{E_0} = \exp\left[-\left(\frac{t}{\tau^*}\right)^{\beta}\right] \quad \text{(Eqn. 1)}$$

where $\tau^*$ is the characteristic relaxation time and $\beta$ ($0 < \beta \leq 1$) is the stretching exponent that characterizes the breadth of the relaxation distribution. Using $\tau^*$ and $\beta$, the average relaxation time, $\langle\tau\rangle$, may be calculated as follows (Eqn. 2):[140]

$$\langle\tau\rangle = \frac{\tau^* \, \Gamma(1/\beta)}{\beta} \quad \text{(Eqn. 2)}$$

where Γ represents the gamma function. Table 4 displays the $\tau^*$, $\beta$, and $\langle\tau\rangle$ values at each temperature tested for each EOC CAN. The stretching exponent, $\beta$, ranges from 0.23 to 0.55 for EOC CANs, notably lower than most values reported for relaxation in polyolefin[101,103] and other CANs.[59,82,87,90,138,141] $\beta$ values this low can be attributed to contributions from trapped loops and entanglements of chains in the CANs.[103,142,143] For all EOC CANs, $\beta$ values increase as temperature increases which, at least in part, may be attributed to cross-link density decreasing with increasing temperature, leading to less heterogeneous networks and less breadth in relaxation distributions.[144]

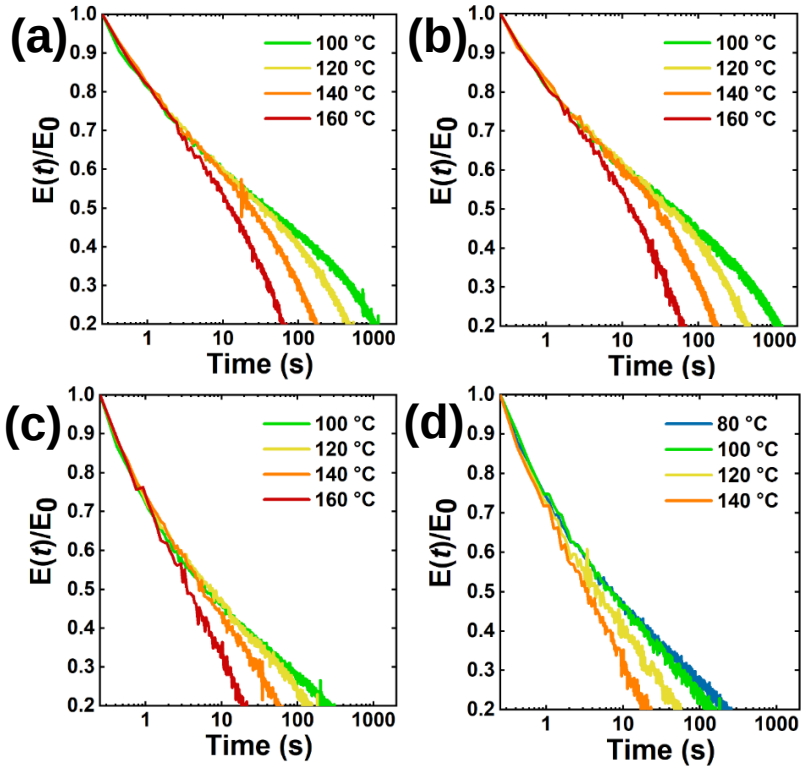


**Figure 4.** Normalized stress relaxation ($E(t)$ relative to $E$ at $t$ = 0 s) curves at various temperatures for (a) EOC CAN-30-1, (b) EOC CAN-38-1, (c) EOC CAN-45-1, and (d) EOC CAN-38-5.

We expected that as temperature increased, relaxation times would decrease, as the dissociation of the BTMA cross-links will be temperature dependent and occur at faster rates at higher temperatures. These expectations were met, as relaxation times decreased with increasing temperature for all EOC CANs. Average stress relaxation times generally decreased with decreasing cross-link density, a trend that has been observed previously for CANs systems of varying cross-link density.[64,145-147] We observed that EOC CAN-30-1 has the longest relaxation times at each temperature. EOC CAN-38-1 followed with the next longest relaxation times at each temperature. Interestingly, EOC CAN-45-1 has shorter relaxation times at each temperature compared to EOC CAN-38-1 despite the two EOC CANs having cross-link densities within error of one another. Lastly, EOC CAN-38-5 exhibited the shortest relaxation times at each temperature, corresponding to it having the lowest cross-link density of the four EOC CANs. We note that some

CAN systems have displayed increasing stress relaxation times or no trend in stress relaxation time with decreasing cross-link density,[148-150] and further study into the mechanisms governing stress relaxation in EOC CANs made from various EOCs is warranted.

**Table 4.** Characteristic relaxation times, stretching exponents, average relaxation times, and KWW decay function fits as a function of temperature for EOC CANs.

| EOC CAN | *T* (°C) | τ* (s) | β | <τ> (s) | $R^2$ |
|---|---|---|---|---|---|
| **EOC CAN-30-1** | 100 | 208 | 0.26 | 3820 | 0.98 |
| | 120 | 123 | 0.32 | 869 | 0.98 |
| | 140 | 59 | 0.42 | 170 | 0.98 |
| | 160 | 26 | 0.49 | 55 | 0.99 |
| **EOC CAN-38-1** | 100 | 234 | 0.28 | 2960 | 0.97 |
| | 120 | 132 | 0.34 | 716 | 0.98 |
| | 140 | 63 | 0.45 | 160 | 0.98 |
| | 160 | 27 | 0.52 | 49 | 0.99 |
| **EOC CAN-45-1** | 100 | 33 | 0.23 | 1330 | 0.98 |
| | 120 | 29 | 0.30 | 280 | 0.98 |
| | 140 | 17 | 0.39 | 61 | 0.98 |
| | 160 | 8 | 0.54 | 14 | 0.99 |
| **EOC CAN-38-5** | 80 | 34 | 0.25 | 730 | 0.98 |
| | 100 | 30 | 0.34 | 160 | 0.97 |
| | 120 | 14 | 0.40 | 48 | 0.98 |
| | 140 | 7.6 | 0.55 | 13 | 0.98 |
| | 160 | < 1 | -- | < 1 | -- |

The $\langle\tau\rangle$ values for the EOC CANs were fitted to the Arrhenius equation to obtain values of stress relaxation activation energy, $E_{a,\tau}$. Figure 5 shows the Arrhenius fits of $\ln(\langle\tau\rangle)$ vs. $1000/T$ plots for each EOC CAN. EOC CAN-30-1, EOC CAN-38-1, and EOC CAN-45-1 exhibit similar $E_{a,\tau}$ values of 96 ± 3, 93 ± 2, and 102 ± 2 kJ/mol, respectively, when fitting stress relaxation data across 100 to 160 °C. These values are nearly within error of one another, and they align with previously reported bond dissociation energies of dialkylamino disulfide and polysulfide bonds in BiTEMPS and BiTEMPS-related molecules.[83,125] It is also notable that these $E_{a,\tau}$ values are similar in magnitude to previously reported stress relaxation and creep activation energies of CANs synthesized with dialkylamino disulfide chemistry as the dissociative dynamic chemistry.[87,88] To obtain an $E_{a,\tau}$ value for EOC CAN-38-5, 80 °C was used as a testing temperature as stress

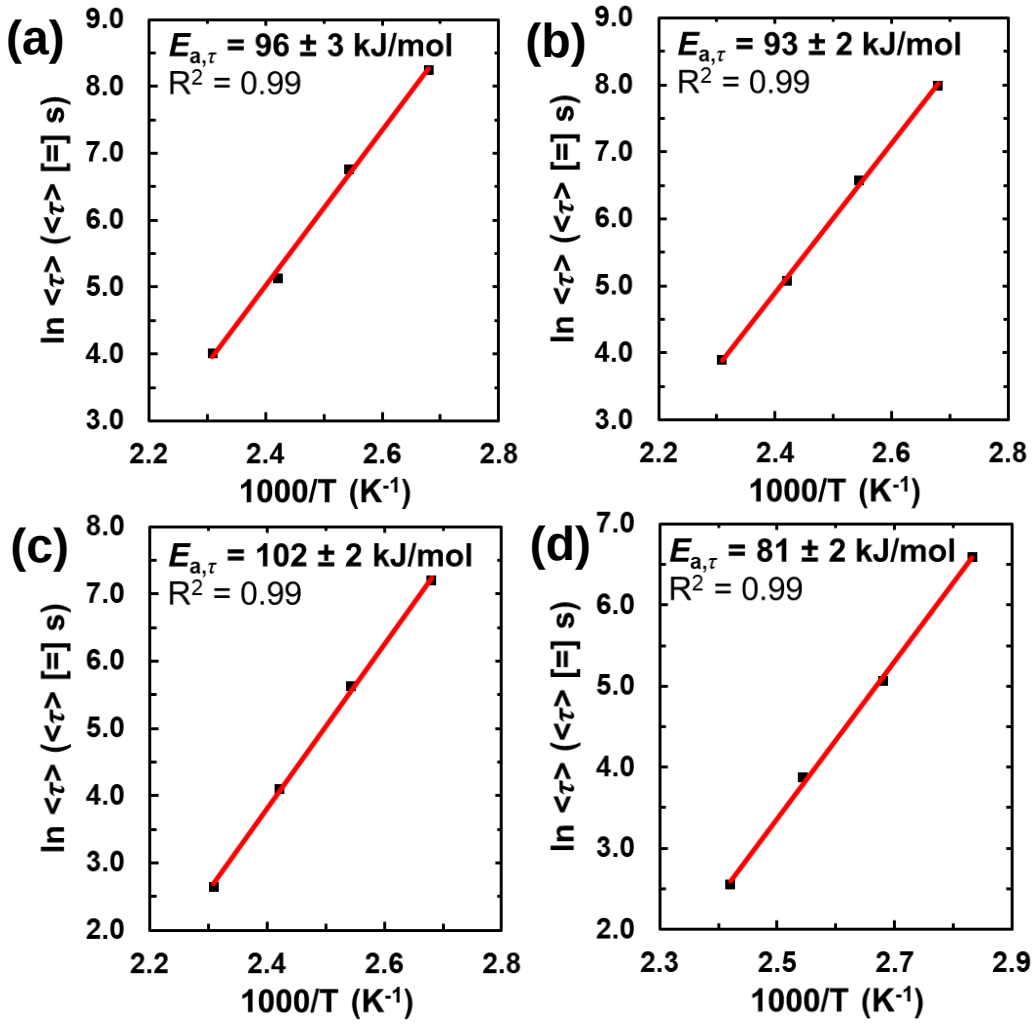


**Figure 5.** Arrhenius apparent activation energies of stress relaxation associated with average relaxation times for (a) EOC CAN-30-1, (b) EOC CAN-38-1, (c) EOC CAN-45-1, and (d) EOC CAN-38-5.

relaxation was too fast at 160 °C to incorporate into an Arrhenius fit. When fitting stress relaxation data across 80 to 140 °C, EOC CAN-38-5 exhibits a slightly lower $E_{a,\tau}$ of 81 ± 2 kJ/mol. While EOC CAN-38-5 showed the steepest loss in cross-link density with increasing temperature by DMA, indicating the strongest temperature dependence of the EOC CANs, EOC CAN-38-5 exhibits the smallest $E_{a,\tau}$ of the EOC CANs. These seemingly contradictory results can be explained by its barely percolated network architecture. In applying a constant strain of 3% to the weakly cross-linked EOC CAN-38-5, motion of the loose cross-links aid in relaxing stress in

tandem with the BTMA dynamic chemistry. Thus, the $E_{a,\tau}$ of EOC CAN-38-5 is strongly contributed to not only by the dissociative dynamic chemistry but also by the viscoelasticity of the loose network itself. This results in both the lowest $E_{a,\tau}$ and the steepest loss in cross-link density with increasing temperature exhibited by EOC CAN-38-5 relative to other EOC CANs.

**3.4. Reprocessing and Property Recovery of EOC CANs.** It is worth investigating whether EOC CANs may be reprocessed into healed EOC CANs given that they are capable of dialkylamino disulfide dynamic chemistry at high temperatures that should enable their reprocessability. As a control study, we first attempted to reprocess EOCXs by cutting 1st-molded EOCXs and compression molding the pieces at 180 °C for 5 min. We were unable to reprocess any EOCXs, as the cut pieces were unable to be molded into healed films. Instead, compression molding EOCXs resulted in unhealed, cracked films; pictures depicting the reprocessing failure of EOCX-38-1 are given in Figure 6 as an example. In contrast, by cutting 1st-molded EOC CANs and compression molding the pieces at 180 °C for 5 min, we were able to reprocess our EOC CANs into fully healed 2nd-molded samples. We also obtained fully healed 3rd-molded samples by reprocessing 2nd-molded samples via another compression molding cycle at the same conditions. Pictures of successfully reprocessed EOC CAN-38-1 are given in Figure 6; other reprocessed EOC CANs may be seen in Figure S14. By compression molding EOC CANs into healed, reprocessed films, we aim to recover the cross-link densities of the original materials within error.

To assess the recovery of cross-link density after reprocessing each EOC CAN, we employed DMA and compared the *E'* rubbery plateau values of 2nd- and 3rd-molded EOC CANs to those of their 1st-molded EOC CANs at several temperatures within the rubbery plateaus. As depicted in Figure 7, the *E'* rubbery plateaus of each 2nd- and 3rd-molded EOC CAN overlap well with the respective *E'* rubbery plateaus of their 1st-molded samples. (Figure S15 displays corresponding tan $\delta$ data as a function of temperature.) The *E'* values listed in Table S3 as a function of temperature also demonstrate that the reprocessed EOC CANs exhibit *E'* values either within error or slightly larger than those of their 1st-molded EOC CAN samples. Any slight increase in *E'* when reprocessing a 1st-molded EOC CAN into a 2nd-molded EOC CAN likely occurred from additional,

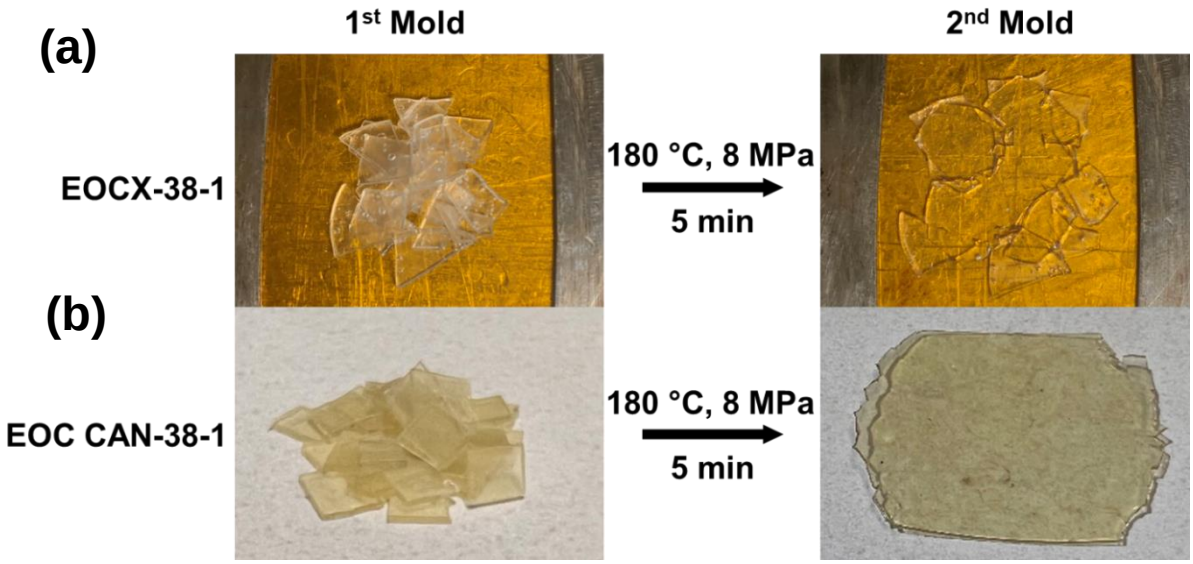


**Figure 6.** (a) Failed reprocessing attempt of 1st-molded EOCX-38-1 that leads to an unhealed, cracked film. (b) Successful reprocessing of 1st-molded EOC CAN-38-1 by cutting and compression molding (180 °C, 8 MPa, 5 min) pieces into healed films (2nd-molded samples). A reprocessing step to prepare 3rd-molded samples was performed similarly. Reprocessings of other EOC CANs are shown in Figure S14.

small amounts of cross-linking that were not completed during initial compression molding to obtain 1st-molded EOC CANs. In fully recovering *E'* at several temperatures within the rubbery plateaus of each reprocessed EOC CAN, we confirm that all of our EOC CANs are reprocessable and fully recovered their cross-link densities after multiple compression molding cycles. The EOC CANs also fully reproduced their room-temperature tensile properties within experimental uncertainty after two reprocessings (Figure S11 and Table S5).

We used DSC to characterize the recovery of thermal properties after reprocessing EOC CANs. Initially, cross-linking EOCs resulted in crystallinity decreases in both EOCXs and EOC CANs relative to precursor EOCs (Table S1). This was expected as cross-linking will disrupt the formation of thicker crystals, thereby leading to decreased crystallinity.[88,151] Melting transitions also shifted to lower temperature ranges in EOCXs and EOC CANs relative to EOCs as a result of cross-linking. After being reprocessed, 2nd- and 3rd-molded EOC CANs exhibit crystallinities and melt transition ranges very similar to those of their 1st-molded samples. Evidenced by DMA,

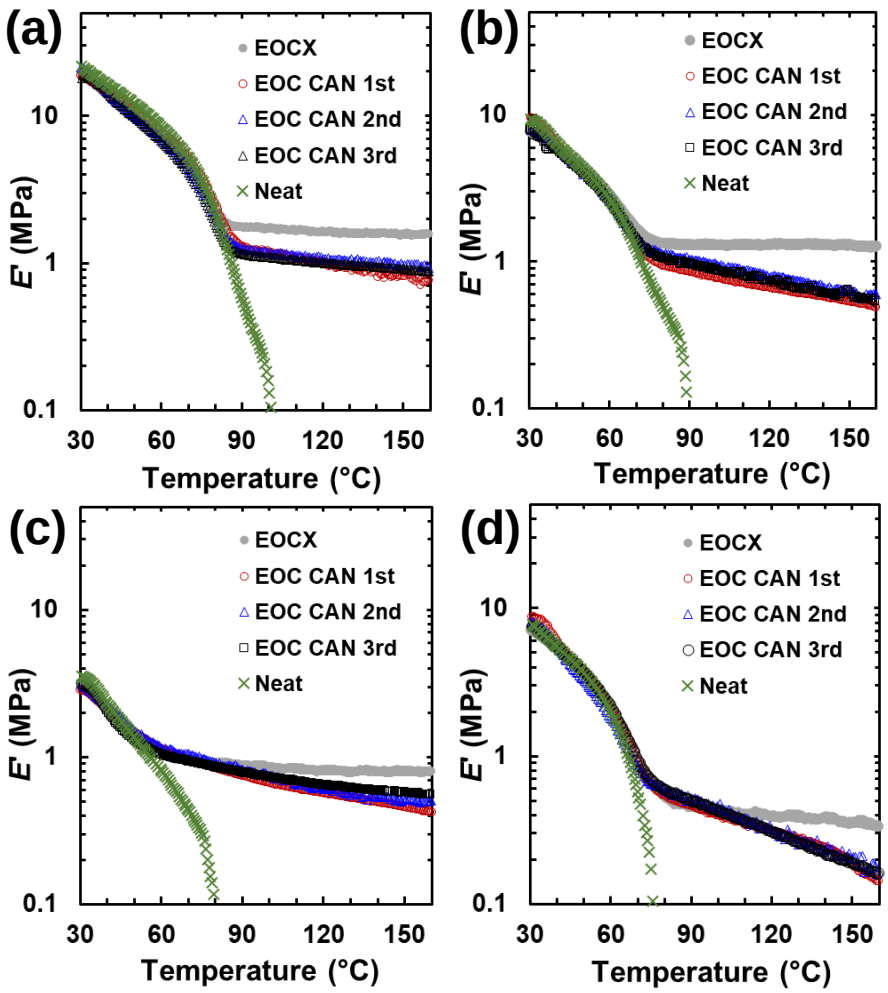


**Figure 7.** Tensile storage modulus (*E*') as a function of temperature and molding of EOC CANs made from (a) EOC-30-1, (b) EOC-38-1, (c) EOC-45-1, and (d) EOC-38-5 with their corresponding EOCXs and neat counterparts.

tensile testing, and DSC data, it is clear that all EOC CANs show full recovery of their thermomechanical properties such as cross-link density and crystallinity after two successive reprocessing cycles. We attribute this excellent reprocessability to the presence of the dynamic sulfur bonds in BTMA that reversibly dissociate into stable sulfur-based radicals at high temperature. Through cross-linking with BTMA, EOC CANs are robustly cross-linked at service

temperatures yet able to gain substantial local chain motion at high temperatures as a result of BTMA chemistry, facilitating their fast (re)processing and recovery of their original properties.

To assess the compatibility of EOC CANs with extrusion reprocessing, we conducted an extrusion experiment on EOC CAN-38-1 in an Xplore MC 40 micro compounder. EOC CAN-38-1 was cured via compression molding at 180 °C and 40000 psi for 15 min before it was cut into pieces. 15-20 g of the CAN were fed into the hopper of the micro compounder. The EOC CAN-38-1 was circulated for 5 min at 200 °C and 25 rpm before being extruded. The extrudate had surface cracks from melt fracture during extrusion (Figure S16). This proof-of-concept experiment demonstrates the compatibility of this dynamic chemistry in EOC CANs with extrusion reprocessing at temperatures upwards of 200 °C. These results warrant further study of EOC CAN property recovery after extrusion and the range of conditions amenable to EOC CAN extrusion as well as their reprocessing potential via injection molding.

We envision conducting future work on trends in creep properties[59,78] in EOC CANs as well as producing EOC CANs with other dynamic chemistries such as associative chemistries. Considering the use of ethylene-based materials like EOCs in nanocomposite and foam formulations,[18] further studies are warranted on reprocessable ethylene-based CAN nanocomposites[138,141,152] and foams[120,153] using our approach with dialkylamino disulfide dynamic chemistry. This work opens the door to extending our methods further to produce CANs from other polymers with limited research in CAN technology. Unsaturated polymers, e.g., EPDM, styrene-butadiene rubber, polyisoprene, and unsaturated polyester resins, are often permanently cross-linked for use in rubber tires, shoe soles, wind turbine blades, and more.[154] Dynamically cross-linking these polymers by exclusively radical-based methods is a promising route to synthesize recyclable versions of their cross-linked commercial products and can contribute to making broadly based polymer recycling[155,156] a reality.

## 4. Conclusions

We permanently and dynamically cross-linked a series of random ethylene/1-octene

copolymers into EOC networks and EOC covalent adaptable networks by free-radical methods. All EOCXs were synthesized with 1 wt% DCP. All EOC CANs were synthesized with 1 wt% DCP and 5 wt% BiTEMPS methacrylate, a cross-linker capable of dialkylamino disulfide dynamic chemistry that is dissociative in nature and enables the dynamic cross-links to cleave into stable sulfur-centered radicals at high temperature.[83,84,128,131] Thereby, EOC CANs are robustly cross-linked like EOCXs at service temperatures but may be processed at high temperatures from the dissociating cross-links. The dissociative dynamic character of the cross-links in EOC CANs was confirmed by their declining temperature-dependent *E'* rubbery plateaus.[85,87,88]

For the first time, we studied the effects of 1-octene content and MFI in precursor EOCs on the thermomechanical properties of both EOCXs and EOC CANs. With increasing 1-octene at constant MFI, we confirmed that cross-link density generally decreases in EOCXs and EOC CANs. We found little difference in EOC CAN cross-link density when increasing 1-octene content beyond 38 wt%. We observed that increasing MFI, or decreasing weight-average molecular weight, in precursor EOCs of nearly constant 1-octene content decreases their propensities to cross-link, resulting in decreased cross-link densities in both EOCXs and EOC CANs.[41,133] EOCXs exhibited larger cross-link densities than their EOC CAN counterparts as evidenced by *E'* rubbery plateau magnitudes and gel contents. We quantified the *E'* losses in EOC CANs with increasing temperature and found that decreasing cross-link density in EOC CANs leads to greater decreases in normalized *E'*, and therefore cross-link density, with increasing temperature. This correlation reflects that barely percolated EOC CANs are more susceptible to losing their percolated network architectures because of small fractional losses of dynamic cross-links during their increased dissociation at increasing temperatures. We further demonstrated that increasing cross-link density in EOC CANs resulted in longer stress relaxation times at all temperatures. Arrhenius stress relaxation activation energies, $E_{a,\tau}$ values, of EOC CANs with an MFI of 1 range reflect previously reported BiTEMPS-related bond dissociation energies as well as activation energies of creep and stress relaxation in other BTMA-based CANs.[83,87,88,125]

We confirm that EOC CANs may be reprocessed by compression molding at 180 °C for 5

min into healed films, whereas their EOCX counterparts cannot. All EOC CANs fully recover their cross-link densities and associated thermomechanical properties by DMA and DSC after two successive reprocessing cycles. In total, we report a simple method, an extension of our previous work involving BTMA-based PE CANs,[88] to prepare not only EOCXs but also several robustly cross-linked and reprocessable EOC CANs. We also addressed the impact of 1-octene content and MFI in EOCs on the properties of the resulting cross-linked EOCs and identified some limits to the EOCs that would result in robust EOCXs and EOC CANs.

## Conflicts of Interest

Two U.S. patent applications have been filed that are related to the research described in this manuscript.

## Supporting Information

Alternative BTMA synthesis, schematic of possible chemistries during EOC CAN synthesis, rheological study data, additional DMA and DSC data of EOCs, EOCXs, EOC CANs and PEC, FTIR spectra and calibration curves, stress-elongation and creep curves, and images of processed EOC CANs by compression molding and extrusion.

## Acknowledgments

This research was supported by the University Partnership Initiative between Northwestern University and The Dow Chemical Company. We also gratefully acknowledge the support from an NSF Graduate Research Fellowship (L.M.F.) and Northwestern University via discretionary funds associated with a Walter P. Murphy Professorship (J.M.T.).

## References

1 F. M. Mirabella and A. Bafna, *J. Polym. Sci. Part B: Polym. Phys.*, 2002, **40**, 1637-1643.

2 D. Li, L. Zhou, X. Wang, L. He and X. Yang, *Materials*, 2019, **12**, 1746.

3 M. Fukuoka, T. Aya, H. Saito, S. Ichihara and H. Sano, *Polym. J.*, 2006, **38**, 542-547.

4 L. Wild, T. Ryle, D. Knobeloch and I. Peat, *J. Polym. Sci.: Polym. Phys. Ed.*, 1982, **20**, 441-455.

5 Z. Guan, P. Cotts, E. McCord and S. McLain, *Science*, 1999, **283**, 2059-2062.

6 P. M. Wood-Adams, J. M. Dealy, A. W. Degroot and O. D. Redwine, *Macromolecules*, 2000, **33**, 7489-7499.

7 D. J. Arriola, E. M. Carnahan, P. D. Hustad, R. L. Kuhlman and T. T. Wenzel, *Science*, 2006, **312**, 714-719.

8 R. Quijada, J. Dupont, M. S. L. Miranda, R. B. Scipioni and G. B. Galland, *Macromol. Chem. Phys.*, 1995, **196**, 3991-4000.

9 J. D. Kim and J. B. Soares, *J. Polym. Sci. Part A: Polym. Chem.*, 2000, **38**, 1427-1432.

10 C. Li Pi Shan, J. B. Soares and A. Penlidis, *J. Polym. Sci. Part A: Polym. Chem.*, 2002, **40**, 4426-4451.

11 P. S. Chum, W. J. Kruper and M. J. Guest, *Adv. Mater.*, 2000, **12**, 1759-1767.

12 J. C. Stevens, F. J. Timmers, D. R. Wilson, G. F. Schmidt, P. N. Nickias, R. K. Rosen, G. W. Knight and S. Y. Lai (The Dow Chemical Company). Eur. Pat. EP416815A2, 1991.

13 M. Terano and K. Soga, *Catalyst design for tailor-made polyolefins*, Elsevier, 1994.

14 S. Bensason, J. Minick, A. Moet, S. Chum, A. Hiltner and E. Baer, *J. Polym. Sci. Part B: Polym. Phys.*, 1996, **34**, 1301-1315.

15 S. Bensason, E. Stepanov, S. Chum, A. Hiltner and E. Baer, *Macromolecules*, 1997, **30**, 2436-2444.

16 P. Svoboda, D. Svobodova, P. Mokrejs, V. Vasek, K. Jantanasakulwong, T. Ougizawa and T. Inoue, *Polymer*, 2015, **81**, 119-128.

17 P. Svoboda, S. Poongavalappil, R. Theravalappil, D. Svobodova and P. Mokrejs, *Polym. Int.*, 2013, **62**, 184-189.

18 Y. Zhao, Y. Ma, Y. Xiong, T. Qin, Y. Zhu, H. Deng, J. Qin, X. Shi and G. Zhang, *Polymer*, 2022, **254**, 125075.

19 K. G. Kummer, J. M. Rego and S. Wu, *Plast. Eng.*, 2013, **69**, 14-22.

20 S. M. Lai, Y. J. Chen and B. Y. Yu, *J. Appl. Polym. Sci.*, 2021, **138**, 51238.

21 S.-M. Lai, S.-Y. F. Jiang, H.-C. Chou, T.-Y. Lin, Y.-E. Wei and B.-Y. Yu, *Polym. Test.*, 2021, **102**, 107333.

22 Y. Li, Y. Liu, P. Gong, Y. Niu, C. B. Park and G. Li, *Ind. Eng. Chem. Res.*, 2022, **61**, 9735-9744.

23 A. Maimaitiming, X. Sun, Y. Lu, G. Wu, Y. Men, X. Dong and Y. Tang, *Composit. Part B: Eng.*, 2022, **246**, 110283.

24 H. y. Lee, D. H. Kim and Y. Son, *J. Appl. Polym. Sci.*, 2007, **103**, 1133-1139.

25 B. Yuan, X. Chen and B. He, *J. Vinyl. Addit. Technol.*, 2008, **14**, 45-54.

26 R. R. Babu, N. K. Singha and K. Naskar, *J. Appl. Polym. Sci.*, 2009, **113**, 1836-1852.

27 M. W. Bodley and J. S. Parent, *Polym. Eng. Sci.*, 2018, **58**, 1999-2007.

28 M. Li, Y. Wang, C. Shen and S. Gao, *J. Elastom. Plast.*, 2022, **54**, 209-224.

29 Z. Wang, X. Cheng and J. Zhao, *Mater. Chem. Phys.*, 2011, **126**, 272-277.

30 H. Le, M. Schoß, S. Ilisch, U. Gohs, G. Heinrich, T. Pham and H.-J. Radusch, *Polymer*, 2011, **52**, 5858-5866.

31 T. Chatterjee, A. B. Bhattacharya, S. Pal and K. Naskar, *Polym. Eng. Sci.*, 2021, **61**, 562-575.

32 Y.-X. Wang, C.-C. Wang, Y. Shi, L.-Z. Liu, N. Bai and L.-F. Song, *Polymers*, 2021, **14**, 139.

33 K. Naskar, S. Mohanty and G. Nando, *J. Appl. Polym. Sci.*, 2007, **104**, 2839-2848.

34 W. Wang, W. Gong and B. Zheng, *J. Vinyl. Addit. Technol.*, 2016, **22**, 61-71.

35 S. Dutta, S. Sengupta, J. Chanda, A. Das, S. Wiessner, S. S. Ray and A. Bandyopadhyay, *Polym. Test.*, 2020, **83**, 106374.

36 U. Basuli, T. Chaki and K. Naskar, *J. Appl. Polym. Sci.*, 2008, **108**, 1079-1085.

37 R. Padmanabhan, K. Naskar and G. B. Nando, *Polym. Plast. Technol. Eng.*, 2017, **56**, 276-295.

38 H.-T. Liao and C.-S. Wu, *Polym. Plast. Technol. Eng.*, 2003, **42**, 1-16.

39 K. Sirisinha and D. Meksawat, *J. Appl. Polym. Sci.*, 2004, **93**, 1179-1185.

40 C. Jiao, Z. Wang, Z. Gui and Y. Hu, *Eur. Polym. J.*, 2005, **41**, 1204-1211.

41 A. Msakni, P. Chaumont and P. Cassagnau, *Polym. Eng. Sci.*, 2006, **46**, 1530-1540.

42 J. Nicolas, J. A. Ressia, E. M. Valles, J. Merino and J. Pastor, *J. Appl. Polym. Sci.*, 2009, **112**, 2691-2700.

43 P. Svoboda, S. Poongavalappil, R. Theravalappil, D. Svobodova, P. Mokrejs, K. Kolomaznik, T. Ougizawa and T. Inoue, *J. Appl. Polym. Sci.*, 2011, **121**, 521-530.

44 Y. X. Wang, Y. Shi, C. C. Wang, J. H. Cheng, Y. Wang, W. J. Shao and L. Z. Liu, *J. Appl. Polym. Sci.*, 2021, **138**, 50651.

45 A. Lendlein and S. Kelch, *Angew. Chem. Int. Ed.*, 2002, **41**, 2034-2057.

46 R. G. Alamo, B. D. Viers and L. Mandelkern, *Macromolecules*, 1993, **26**, 5740-5747.

47 P. Svoboda, *Polymers*, 2015, **7**, 2522-2534.

48 J. Nicolás, N. Villarreal, I. Gobernado-Mitre, J. C. Merino and J. M. Pastor, *Macromol. Chem. Phys.*, 2003, **204**, 2212-2221.

49 X. Chen, M. A. Dam, K. Ono, A. Mal, H. Shen, S. R. Nutt, K. Sheran and F. Wudl, *Science*, 2002, **295**, 1698-1702.

50 P. Cordier, F. Tournilhac, C. Soulié-Ziakovic and L. Leibler, *Nature*, 2008, **451**, 977-980.

51 R. J. Wojtecki, M. A. Meador and S. J. Rowan, *Nat. Mater.*, 2011, **10**, 14-27.

52 N. J. Van Zee and R. Nicolaÿ, *Prog. Polym. Sci.*, 2020, **104**, 101233.

53 C. J. Kloxin, T. F. Scott, B. J. Adzima and C. N. Bowman, *Macromolecules*, 2010, **43**, 2643-2653.

54 M. Podgórski, B. D. Fairbanks, B. E. Kirkpatrick, M. McBride, A. Martinez, A. Dobson, N. J. Bongiardina and C. N. Bowman, *Adv. Mater.*, 2020, **32**, 1906876.

55 W. Zou, J. Dong, Y. Luo, Q. Zhao and T. Xie, *Adv. Mater.*, 2017, **29**, 1606100.

56 W. Denissen, J. Winne and F. Du Prez, *Chem. Sci.*, 2016, **7**, 30-38.

57 M. Capelot, D. Montarnal, F. Tournilhac and L. Leibler, *J. Am. Chem. Soc.*, 2012, **134**, 7664-7667.

58 Z. Pei, Y. Yang, Q. Chen, Y. Wei and Y. Ji, *Adv. Mater.*, 2016, **28**, 156-160.

59 L. Li, X. Chen, K. Jin and J. M. Torkelson, *Macromolecules*, 2018, **51**, 5537-5546.

60 W. Denissen, G. Rivero, R. Nicolaÿ, L. Leibler, J. M. Winne and F. E. Du Prez, *Adv. Funct. Mater.*, 2015, **25**, 2451-2457.

61 M. M. Obadia, A. Jourdain, P. Cassagnau, D. Montarnal and E. Drockenmuller, *Adv. Funct. Mater.*, 2017, **27**, 1703258.

62 J. J. Lessard, L. F. Garcia, C. P. Easterling, M. B. Sims, K. C. Bentz, S. Arencibia, D. A. Savin and B. S. Sumerlin, *Macromolecules*, 2019, **52**, 2105-2111.

63 Y. Chen, Z. Tang, X. Zhang, Y. Liu, S. Wu and B. Guo, *ACS Appl. Mater. Interfaces*, 2018, **10**, 24224-24231.

64 B. Soman and C. M. Evans, *Soft Matt.*, 2021, **17**, 3569-3577.

65 S. Tajbakhsh, F. Hajiali and M. Maric, *ACS Appl. Polym. Mater.*, 2021, **3**, 3402-3415.

66 J. Deng, X. Kuang, R. Liu, W. Ding, A. C. Wang, Y. C. Lai, K. Dong, Z. Wen, Y. Wang and L. Wang, *Adv. Mater.*, 2018, **30**, 1705918.

67 H. Si, L. Zhou, Y. Wu, L. Song, M. Kang, X. Zhao and M. Chen, *Composit. Part B: Eng.*, 2020, **199**, 108278.

68 L. Li, X. Chen and J. M. Torkelson, *ACS Appl. Polym. Mater.*, 2020, **2**, 4658-4665.

69 D. Montarnal, M. Capelot, F. Tournilhac and L. Leibler, *Science*, 2011, **334**, 965-968.

70 M. Capelot, M. Unterlass, F. Tournilhac and L. Leibler, *ACS Macro Lett.*, 2012.

71 K. K. Oehlenschlaeger, J. O. Mueller, J. Brandt, S. Hilf, A. Lederer, M. Wilhelm, R. Graf, M. L. Coote, F. G. Schmidt and C. Barner-Kowollik, *Adv. Mater.*, 2014, **26**, 3561-3566.

72 J. Bai, H. Li, Z. Shi and J. Yin, *Macromolecules*, 2015, **48**, 3539-3546.

73 L. Polgar, M. Van Duin, A. Broekhuis and F. Picchioni, *Macromolecules*, 2015, **48**, 7096-7105.

74 C. Shao, M. Wang, H. Chang, F. Xu and J. Yang, *ACS Sustain. Chem. Eng.*, 2017, **5**, 6167-6174.

75 X. Xu, S. Ma, S. Wang, B. Wang, H. Feng, P. Li, Y. Liu, Z. Yu and J. Zhu, *Macromol. Rap. Comm.*, 2022, **43**, 2100777.

76 H. Otsuka, *Polym. J.*, 2013, **45**, 879-891.

77 K. Jin, L. Li and J. M. Torkelson, *Adv. Mater.*, 2016, **28**, 6746-6750.

78 L. Li, X. Chen, K. Jin, M. Bin Rusayyis and J. M. Torkelson, *Macromolecules*, 2021, **54**, 1452-1464.

79 H. Ying, Y. Zhang and J. Cheng, *Nat. Comm.*, 2014, **5**, 3218.

80 Y. Zhang, H. Ying, K. R. Hart, Y. Wu, A. J. Hsu, A. M. Coppola, T. A. Kim, K. Yang, N. R. Sottos and S. R. White, *Adv. Mater.*, 2016, **28**, 7646-7651.

81 Q. Zhang, S. Wang, B. Rao, X. Chen, L. Ma, C. Cui, Q. Zhong, Z. Li, Y. Cheng and Y. Zhang, *React. Funct. Polym.*, 2021, **159**, 104807.

82 M. A. Bin Rusayyis and J. M. Torkelson, *ACS Macro Lett.*, 2022, **11**, 568-574.

83 A. Takahashi, R. Goseki and H. Otsuka, *Angew. Chem. Int. Ed.*, 2017, **56**, 2016-2021.

84 A. Takahashi, R. Goseki, K. Ito and H. Otsuka, *ACS Macro Letters*, 2017, **6**, 1280-1284.

85 M. Bin Rusayyis and J. M. Torkelson, *Macromolecules*, 2020, **53**, 8367-8373.

86 S. Kataoka, A. Tsuruoka, D. Aoki and H. Otsuka, *ACS Appl. Polym. Mater.*, 2021, **3**, 888-895.

87 M. A. Bin Rusayyis and J. M. Torkelson, *Polym. Chem.*, 2021, **12**, 2760-2771.

88 L. M. Fenimore, B. Chen and J. M. Torkelson, *J. Mater. Chem. A*, 2022, **10**, 24726-24745.

89 X. Chen, L. Li, K. Jin and J. M. Torkelson, *Polym. Chem.*, 2017, **8**, 6349-6355.

90 L. Li, X. Chen and J. M. Torkelson, *Macromolecules*, 2019, **52**, 8207-8216.

91 X. Chen, S. Hu, L. Li and J. M. Torkelson, *ACS Appl. Polym. Mater.*, 2020, **2**, 2093-2101.

92 S. Hu, X. Chen and J. M. Torkelson, *ACS Sustain. Chem. Eng.*, 2019, **7**, 10025-10034.

93 C. Zhang, X. Wang, D. Liang, H. Deng, Z. Lin, P. Feng and Q. Wang, *J. Mater. Chem. A*, 2021, **9**, 18431-18439.

94 N. S. Purwanto, Y. Chen, T. Wang and J. M. Torkelson, *Polymer*, 2023, 125858.

95 M. Röttger, T. Domenech, R. van Der Weegen, A. Breuillac, R. Nicolaÿ and L. Leibler, *Science*, 2017, **356**, 62-65.

96 F. Caffy and R. Nicolaÿ, *Polym. Chem.*, 2019, **10**, 3107-3115.

97 F. Ji, X. Liu, C. Lin, Y. Zhou, L. Dong, S. Xu, D. Sheng and Y. Yang, *Macromol. Mater. Eng.*, 2019, **304**, 1800528.

98 G. P. Kar, M. O. Saed and E. M. Terentjev, *J. Mater. Chem. A*, 2020, **8**, 24137-24147.

99 M. Maaz, A. Riba-Bremerch, C. Guibert, N. J. Van Zee and R. Nicolaÿ, *Macromolecules*, 2021, **54**, 2213-2225.

100 R. G. Ricarte, F. Tournilhac and L. Leibler, *Macromolecules*, 2018, **52**, 432-443.

101 J. Tellers, R. Pinalli, M. Soliman, J. Vachon and E. Dalcanale, *Polym. Chem.*, 2019, **10**, 5534-5542.

102 Z. Wang, Y. Gu, M. Ma, Y. Liu and M. Chen, *Macromolecules*, 2021, **54**, 1760-1766.

103 A. Zych, R. Pinalli, M. Soliman, J. Vachon and E. Dalcanale, *Polymer*, 2020, **199**, 122567.

104 M. O. Saed, X. Lin and E. M. Terentjev, *ACS Appl. Mater. Interfaces*, 2021, **13**, 42044-42051.

105 S. Wang, S. Ma, J. Qiu, A. Tian, Q. Li, X. Xu, B. Wang, N. Lu, Y. Liu and J. Zhu, *Green Chem.*, 2021, **23**, 2931-2937.

106 Y. Liu, Z. Tang, J. Chen, J. Xiong, D. Wang, S. Wang, S. Wu and B. Guo, *Polym. Chem.*, 2020, **11**, 1348-1355.

107 Z. He, H. Niu, N. Zheng, S. Liu and Y. Li, *Polym. Chem.*, 2019, **10**, 4789-4800.

108 F. Yang, L. Pan, Z. Ma, Y. Lou, Y. Li and Y. Li, *Polym. Chem.*, 2020, **11**, 3285-3295.

109 A. Breuillac, A. Kassalias and R. Nicolaÿ, *Macromolecules*, 2019, **52**, 7102-7113.

110 Y. Yang, L. Huang, R. Wu, Z. Niu, W. Fan, Q. Dai, L. Cui, J. He and C. Bai, *ACS Appl. Mater. Interfaces*, 2022, **14**, 3344-3355.

111 Q. Huang, Z. Tang, D. Wang, S. Wu and B. Guo, *ACS Macro Lett.*, 2021, **10**, 231-236.

112 C. A. Tretbar, J. A. Neal and Z. Guan, *J. Am. Chem. Soc.*, 2019, **141**, 16595-16599.

113 H. Zhang, D. Wang, W. Liu, P. Li, J. Liu, C. Liu, J. Zhang, N. Zhao and J. Xu, *J. Polym. Sci. Part A: Polym. Chem.*, 2017, **55**, 2011-2018.

114 M. Ahmadi, A. Hanifpour, S. Ghiassinejad and E. van Ruymbeke, *Chem. Mater.*, 2022, **34**, 10249-10271.

115 H. Verhoogt, J. Vachon and J. Tellers, US Pat., US20220332932, 2019.

116 L. Cheng, W. Yu, W. You and S. Liu, Cn. Pat., CN112126150, 2020.

117 Y. Zhao, J. Li, T. Qin, Y. Xiong, Y. Ma and C. Jiang, Cn. Pat., CN114456530, 2022.

118 W.-Y. Wang, X.-J. Zha, R.-Y. Bao, K. Ke, Z.-Y. Liu, M.-B. Yang and W. Yang, *J. Polym. Res.*, 2021, **28**, 210.

119 Y. Xiao, P. Liu, W.-J. Wang and B.-G. Li, *Macromolecules*, 2021, **54**, 10381-10387.

120 L. Cheng, B. Li, S. Liu and W. Yu, *Polymer*, 2021, **232**, 124159.

121 Z. Xu, S. Meng, D.-W. Wei, R.-Y. Bao, Y. Wang, K. Ke and W. Yang, *Nanoscale*, 2023, **15**, 5458-5468.

122 L.-M. Peng, Z. Xu, J. Yang, L. Bai, R.-Y. Bao, M.-B. Yang and W. Yang, *Chem. Eng. J.*, 2023, **455**, 140891.

123 Z. Xu, Y.-B. Liu, D.-W. Wei, R.-Y. Bao, Y. Wang, K. Ke and W. Yang, *ACS Appl. Mater. Interfaces*, 2023, **15**, 12423-12433.

124 Technical data sheets, courtesy of The Dow Chemical Company.

125 M. Aiba, T.-A. Koizumi, M. Futamura, K. Okamoto, M. Yamanaka, Y. Ishigaki, M. Oda, C. Ooka, A. Tsuruoka and A. Takahashi, *ACS Appl. Polym. Mater.*, 2020, **2**, 4054-4061.

126 M. Marić and C. W. Macosko, *Polym. Eng. Sci.*, 2001, **41**, 118-130.

127 S. Alapati, J. T. Meledath and A. Karmarkar, *IET Sci. Meas. Technol.*, 2014, **8**, 60-68.

128 J. Bennett, H. Sieper and P. Tavs, *Tetrahedron*, 1967, **23**, 1697-1699.

129 W. C. Danen and D. D. Newkirk, *J. Am. Chem. Soc.*, 1976, **98**, 516-520.

130 B. Maillard and K. Ingold, *J. Am. Chem. Soc.*, 1976, **98**, 520-523.

131 S. Nevejans, N. Ballard, J. I. Miranda, B. Reck and J. M. Asua, *Phys. Chem. Chem. Phys.*, 2016, **18**, 27577-27583.

132 P. J. Flory, *Principles of Polymer Chemistry*, Cornell University Press, 1953.

133 M. Lazar, R. Rado and J. Rychlý, *Crosslinking of Polyolefins*, Springer, 1990.

134 M. Rätzsch, M. Arnold, E. Borsig, H. Bucka and N. Reichelt, *Prog. Polym. Sci.*, 2002, **27**, 1195-1282.

135 H. Hinsken, S. Moss, J.-R. Pauquet and H. Zweifel, *Polym. Degrad. Stab.*, 1991, **34**, 279-293.

136 M. F. Diop and J. M. Torkelson, *Polymer*, 2013, **54**, 4143-4154.

137 M. K. McBride, B. T. Worrell, T. Brown, L. M. Cox, N. Sowan, C. Wang, M. Podgorski, A. M. Martinez and C. N. Bowman, *Annu. Rev. Chem. Biomol. Eng.*, 2019, **10**, 175-198.

138 X. Chen, L. Li, T. Wei, D. C. Venerus and J. M. Torkelson, *ACS Appl. Mater. Interfaces*, 2018, **11**, 2398-2407.

139 Q. Ge, K. Yu, Y. Ding and H. J. Qi, *Soft Matt.*, 2012, **8**, 11098-11105.

140 J. C. Hooker and J. M. Torkelson, *Macromolecules*, 1995, **28**, 7683-7692.

141 S. Hu, X. Chen, M. A. Bin Rusayyis, N. S. Purwanto and J. M. Torkelson, *Polymer*, 2022, **252**, 124971.

142 A. Hotta, S. Clarke and E. Terentjev, *Macromolecules*, 2002, **35**, 271-277.

143 F. Meng, R. H. Pritchard and E. M. Terentjev, *Macromolecules*, 2016, **49**, 2843-2852.

144 L. E. Porath and C. M. Evans, *Macromolecules*, 2021, **54**, 4782-4791.

145 K. Yu, P. Taynton, W. Zhang, M. L. Dunn and H. J. Qi, *RSC Adv.*, 2014, **4**, 48682-48690.

146 D. J. Fortman, J. P. Brutman, M. A. Hillmyer and W. R. Dichtel, *J. Appl. Polym. Sci.*, 2017, **134**, 44984.

147 Z. Wang, Y. Gu, M. Ma and M. Chen, *Macromolecules*, 2020, **53**, 956-964.

148 Y. Spiesschaert, C. Taplan, L. Stricker, M. Guerre, J. M. Winne and F. E. Du Prez, *Polym. Chem.*, 2020, **11**, 5377-5385.

149 M. Hayashi and R. Yano, *Macromolecules*, 2019, **53**, 182-189.

150 J. S. A. Ishibashi, I. C. Pierce, A. B. Chang, A. Zografos, B. M. El-Zaatari, Y. Fang, S. J. Weigand, F. S. Bates and J. A. Kalow, *Macromolecules*, 2021, **54**, 3972-3986.

151 S. M. Tamboli, S. T. Mhaske and D. D. Kale, *Indian J. Chem. Technol.*, 2004, **11**, 853-864.

152 B. Zhao, G. Hang, L. Li and S. Zheng, *Mater. Today Chem.*, 2022, **24**, 100759.

153 L. Cheng, S. Liu and W. Yu, *Polymer*, 2021, **222**, 123662.

154 A. K. Bhowmick and H. Stephens, *Handbook of Elastomers*, CRC Press, 2000.

155 K. Khait and J. M. Torkelson, *Polym. Plast. Technol. Eng.*, 1999, **38**, 445-457.

156 M. Okan, H. M. Aydin and M. Barsbay, *J. Chem. Technol. Biotechnol.*, 2019, **94**, 8-21.